Contrib Mineral Petrol (2006) 151: 1–19
DOI 10.1007/s00410-005-0030-y

ORIGINAL PAPER

**Mei-Fu Zhou · Jun-Hong Zhao · Liang Qi
Wenchao Su · Ruizhong Hu**

Zircon U-Pb geochronology and elemental and Sr–Nd isotope geochemistry of Permian mafic rocks in the Funing area, SW China

Received: 1 March 2005 / Accepted: 3 August 2005 / Published online: 22 November 2005

Abstract Mafic-layered intrusions and sills and spatially associated andesitic basalts are well preserved in the Funing area, SW China. The 258 ± 3 Ma-layered intrusions are composed of fine-grained gabbro, gabbro and diorite. The 260 ± 3 Ma sills consist of undifferentiated diabases. Both the layered intrusions and volcanic rocks belong to a low-Ti group, whereas the diabases belong to a high-Ti group. Rocks of the high-Ti group have FeO, TiO_2 and P_2O_5 higher but MgO and Th/Nb ratios lower than those of the low-Ti group. They have initial $^{87}Sr/^{86}Sr$ ratios (0.706–0.707) lower and εNd (−1.5 to −0.6) higher than the low-Ti equivalents (0.710–0.715 and −9.6 to −4.0, respectively). The high-Ti group was formed from relatively primitive, high-Ti magmas generated by low degrees (7.3 –9.5%) of partial melting of an enriched, OIB-type asthenospheric mantle source. The low-Ti group may have formed from melts derived from an EM2-like, lithospheric mantle source. The mafic rocks at Funing are part of the Emeishan large igneous province formed by a mantle plume at ~260 Ma.

Introduction

The Emeishan flood basalts in SW China and northern Vietnam have a well-constrained Late Middle-Permian (~260 Ma) eruptive age (Yin et al. 1992; Jin and Shang 2000; Ali et al. 2004) and include high-Ti and low-Ti basalts (Xu et al. 2001; Xiao et al. 2003), as well as alkaline rocks such as trachyandesites and trachytes (Ma et al. 2003). These basalts form part of the Emeishan Large Igneous Province (ELIP), which also includes intrusive bodies of sub-volcanic sills/dykes and layered intrusions with a variety of magmatic mineral deposits (Zhong et al. 2002, Zhou et al. 2002c; 2005; Song et al. 2003). If the intrusive bodies were part of the same igneous event that produced the ELIP, one would expect a genetic relationship between them and the extrusive rocks and a similar diversity of composition in these bodies.

The diversity of extrusive and intrusive rocks in many LIPs, such as in Siberia, is explained by variable mantle sources, mantle plume–lithosphere interaction, crustal contamination, fractionation, sulfide saturation, or a combination of these processes (Naldrett et al. 1992; Arndt et al. 1993; 1998; 2003; Lightfoot et al. 1990, 1993, 1994; Fedorenko and Czamanske 1997). There has been no attempt to link the different types of intrusions in the ELIP to one another or to the associated volcanic sequences, thus, factors that controlled the origin and diversity of the ELIP are not well understood.

In the Funing area, east of the ELIP (Fig. 1), abundant mafic intrusions in Carboniferous and Devonian strata are relatively well preserved and are spatially associated with volcanic rocks of the same age (Wu et al. 1963; YBGMR 1990). However, these rocks have traditionally not been included in the ELIP and their genetic relationship with the ELIP elsewhere remains unclear, because their age of emplacement and geochemistry have not been studied in detail.

In this paper we report the first geochronological and geochemical data for mafic rocks in Funing and use these data to examine their age and origin. Zircons from the intrusions were separated and dated using the sensitive high-resolution ion microprobe (SHRIMP) technique. The dating yielded ages of ~260 Ma, similar to the age of the ELIP (Zhou et al. 2002b). The whole-rock major oxides, trace elements and Rb–Sr and Sm–Nd isotopic characteristics of these rocks reveal a considerable compositional diversity. Using these data, an attempt to identify the nature of the mantle sources, the

Communicated by Timothy L. Grove

M.-F. Zhou (✉) · J.-H. Zhao · L. Qi · W. Su · R. Hu
Institute of Geochemistry, Chinese Academy of Sciences, Guiyang, China

M.-F. Zhou
Department of Earth Sciences, University of Hong Kong, Hong Kong, Peoples Republic of China
E-mail: mfzhou@hkucc.hku.hk
Tel.: +852-28578251
Fax: +852-25176912

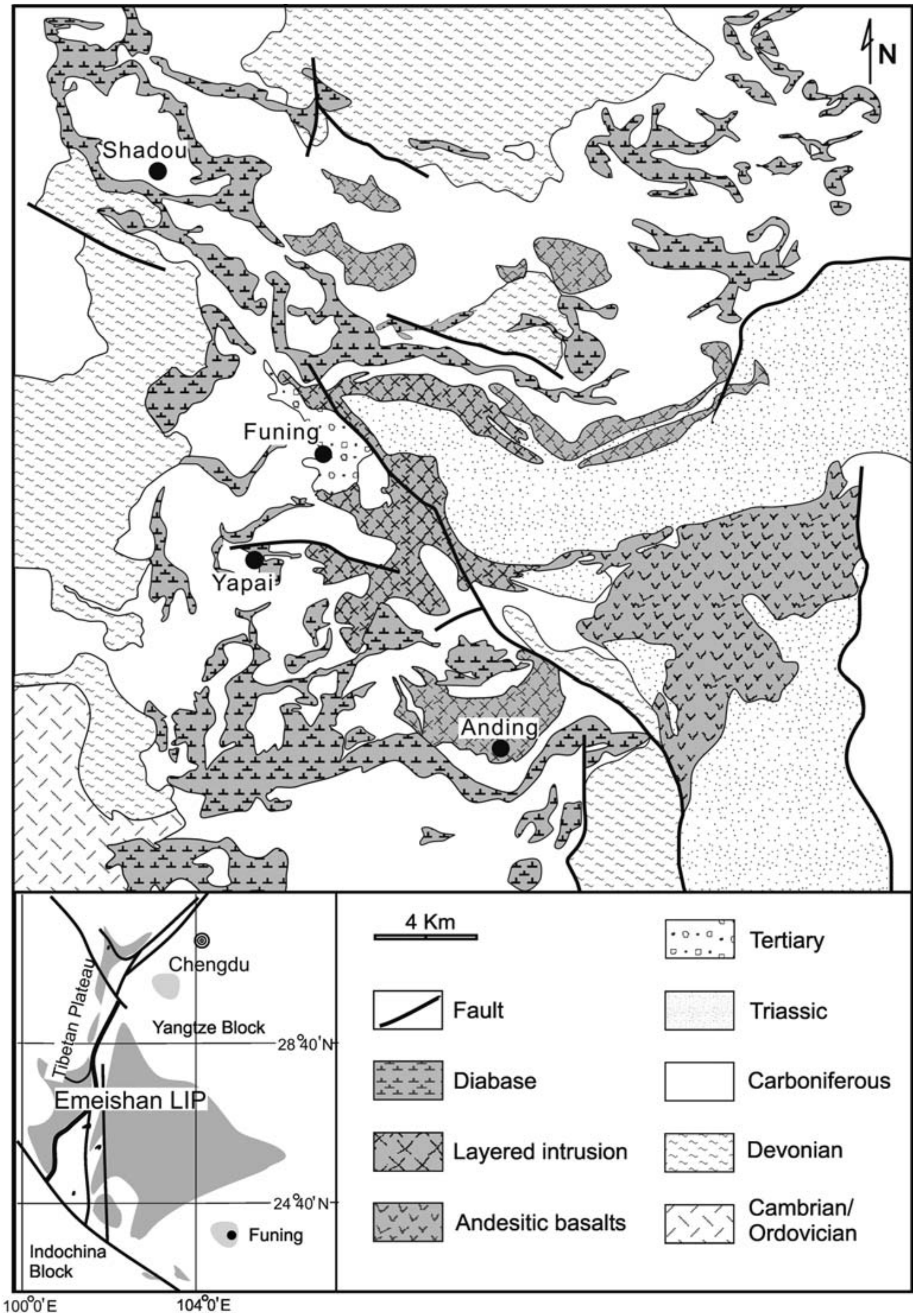

Fig. 1 Geological map of the Funing area, Yunnan Province, SW China (after Wu et al. 1963), showing the distribution of mafic–ultramafic intrusions and volcanic rocks

compositions of parental magmas, and the processes involved in the evolution of these magmas was made.

Geological background

SW China comprises the Yangtze Block to the east, the Tibetan Plateau to the west, and the Indochina Block to the south (Fig. 1). The Yangtze Block consists of a Precambrian basement overlain by stratigraphic sequences ranging from late Mesoproterozoic to upper Jurassic and younger in age. The lower and middle parts of the sequence are basically marine sedimentary rocks, whereas the upper part consists mostly of terrestrial basin deposits (Yan et al. 2003). Along the western margin of the Yangtze Block, there are abundant Neoproterozoic granites and associated metamorphic rocks known as the Kangdian complexes, which were likely uplifted at ~175 Ma (Zhou et al. 2002a). Farther west, in the easternmost part of the Tibetan Plateau, is the

Songpan-Ganze Terrane, which is characterized by a thick (up to more than 10 km) sequence of Late Triassic strata of deep marine origin (Yin and Nie 1996).

Rocks of the ELIP crop out in the eastern part of the Tibetan Plateau and the western part of the Yangtze Block (Fig. 1) and extend over much of SW China and Northern Vietnam (Fig. 1). The ELIP comprises the Emeishan flood basalts and associated mafic–ultramafic and syenitic intrusions. The Emeishan volcanic succession varies in thickness from several hundred meters upto 5 km and includes picrites, tholeiites, and andesitic basalts, all of which are believed to have formed by melting associated with a mantle plume event (Chung and Jahn 1995; Song et al. 2001; Xu et al. 2001; Xiao et al. 2003).

In the western part of the ELIP, the volcanic succession has been strongly deformed, uplifted, and eroded as a result of the Tertiary India-Eurasia collision (Boven et al. 2002; Ali et al. 2004). The distribution of the Late Middle Permian flood basalts on the eastern edge of the Tibetan Plateau indicates that the thick Triassic sedimentary sequence of the Songpan-Ganze Terrane was deposited in a basin that formed during rifting associated with the Emeishan mantle plume (Song et al. 2004). To the southeast, Permian flood basalts are known in Jinping of southern Yunnan, SW China (Xiao et al. 2003), and in Song Da of northern Vietnam (Hanski et al. 2004).

Permian mafic intrusions and basalts in the Funing area (Fig. 1) are exposed in the southeastern part of the Yangtze Block and are relatively well preserved. They are exposed in the cores of anticlines in the South China Mesozoic fold belt (Yan et al. 2003) and are hosted by Paleozoic strata. Because these intrusions are typically unaltered, they provide a rare opportunity to examine the geochemical processes involved in their formation. Mafic intrusions occur either as undifferentiated diabase sills/dykes or layered intrusions (Fig. 1). Several layered intrusions, such as the Anding and Yapai intrusions, cross-cut the host strata, whereas the mafic sills, such as the Shadou sill, are all conformable with the strata. Volcanic rocks crop out extensively in the eastern part of the area (Fig. 1).

Petrography of intrusive and extrusive rocks in Funing

Diabase sills/dykes

The Shadou intrusion, a sill-like body, about 10-km long and 200-m thick (Fig. 1), is intruded comformably into Carboniferous strata. The sill lies in a syncline, in which Middle Carboniferous limestone forms the hanging wall and Lower Carboniferous sandy shales form the footwall. Along the footwall of the intrusion, the sedimentary rocks are metamorphosed to hornfels. The body is composed of diabase, which becomes relatively coarse-grained in the center of the sill. Plagioclase and clinopyroxene are the major minerals but small amounts of olivine occur in the lower parts and magnetite is a common accessory mineral throughout.

Diabases also occur as dykes in Anding and Yapai and are petrographically similar to the Shadou sill.

Layered mafic intrusions

Both the Anding and Yapai intrusions are typical layered intrusions (Fig. 1). The Anding intrusion is 6.5-km long and about 3-km wide with a surface exposure of 15 km^2, and is also intruded into Carboniferous strata. From the base upward it consists of a lower marginal zone, a middle gabbroic zone, and an upper diorite zone. The chilled marginal zone is about 60-m thick; it is composed of fine-grained gabbro and contains abundant xenoliths of the country rock. Patches of skarn are developed locally along the contact. The marginal zone is transitional to the middle gabbroic zone, which is composed mainly of clinopyroxene and plagioclase. In the lower part of the middle zone both orthopyroxene and olivine are present and form olivine-noritic gabbro. Some disseminated sulfide layers in this zone were a major exploration target (Wu et al. 1963). The uppermost zone consists of diorite composed chiefly of plagioclase, amphibole, and minor quartz.

The Yapai intrusion is similar to the Anding intrusion with the same three zones: a lower marginal zone, a middle gabbroic zone, and an upper diorite zone.

Volcanic sequence

The volcanic rocks in the Funing region overlie Carboniferous strata and are overlain unconformably by Triassic sedimentary rocks. They contain abundant xenoliths of plutonic rock derived from the intrusions and of Carboniferous strata. Many of the lava flows have well-developed, nearly vertical, columnar jointing. Sparse layers of tuff and volcanic breccia occur between some flows. The rocks are porphyritic in texture with phenocrysts of plagioclase, clinopyroxene, and sparse olivine set in a fine-grained matrix of the same composition. Chlorite-filled amygdules are present locally.

Analytical methods

SHRIMP zircon analyses

Zircon grains were separated using conventional heavy liquid and magnetic techniques, mounted in epoxy, polished, coated with gold, and photographed in transmitted and reflected light to identify grains for analysis. U–Pb isotopic ratios of zircon separates were measured using the SHRIMP II at the Curtin University of

Technology in Perth, Western Australia, and at the Chinese Academy of Geological Sciences, Beijing, China. In both these laboratories, the measured isotope ratios were reduced off-line using standard techniques (see Claoué-Long et al. 1991). The U–Pb ages were normalized to a value of 564 Ma determined by conventional U–Pb analysis of zircon standards (CZ3 in the Perth lab and SL13 in the Beijing lab). Common Pb was corrected using the methods of Compston et al. (1984). The $^{206}Pb/^{238}U$ and $^{207}Pb/^{235}U$ data were corrected for uncertainties associated with the measurements of the CZ3 or SL13 standards. The $^{207}Pb/^{206}Pb$ ages given in Table 1 are independent of the standard analyses.

Whole-rock geochemical analyses

Samples were collected from the best-exposed and least-altered outcrops. The analyzed samples are believed to be representative of the major lithologies in the intrusions. The samples were cut with a diamond-impregnated brass blade, crushed in a steel jaw crusher that was brushed and cleaned with de-ionized water, and pulverized in agate mortars in order to minimize potential contamination. Major oxides were determined by wavelength-dispersive x-ray fluorescence spectrometry (WD-XRFS) on fused glass beads using a Philips PW2400 spectrometer at the University of Hong Kong. Trace elements, including REE, were determined by inductively coupled plasma mass spectrometry (ICP-MS) of nebulized solutions using a VG Plasma-Quad Excell ICP-MS at the University of Hong Kong after a 2-day closed-beaker digestion using a mixture of HF and HNO_3 acids in high-pressure bombs (Qi et al. 2000). Pure elemental standard solutions were used for external calibration and BHVO-1 and SY-4 were used as reference materials. The accuracies of the XRF analyses are estimated to be ±2% (relative) for major oxides present

Table 1 SHRIMP zircon U-Pb analytical results for the mafic rocks in Funing, SW China

Spot	U	Th	Pb	Th/U	Ages (Ma)							
					$^{206}Pb/^{238}U$	±	$^{207}Pb/^{235}U$	±	$^{207}Pb/^{206}Pb$	±	$^{208}Pb/^{232}Th$	±
Sample FL7 (a diabase from the Shadou sill)												
FL7-1.1	3633	4246	129	1.21	264	9	248	6	122	21	250	7
FL7-2.1	388	354	16.8	0.94	315	10	312	11	275	67	327	11
FL7-3.1	2899	7342	101	2.62	261	12	248	7	186	30	246	7
FL7-4.1	1761	2264	61.4	1.33	258	9	245	7	140	31	250	7
FL7-5.1	379	323	13.9	0.88	269	9	243	15	20	150	257	11
FL7-6.1	1500	2201	53.9	1.52	267	9	250	7	119	45	253	8
FL7-7.1	1441	5247	51.6	3.76	273	18	245	8	76	54	255	7
FL7-9.1	2473	5601	87.6	2.34	265	11	242	6	71	25	253	7
FL7-10.1	4336	5551	159	1.32	271	9	254	6	120	19	263	7
FL7-11.1	2656	7430	93.2	2.89	250	13	240	6	71	32	268	8
FL7-12.1	3587	9250	130	2.66	274	13	249	7	82	30	256	7
FL7-13.1	6343	19489	231	3.17	276	15	255	6	137	17	258	7
FL7-14.1	1891	3286	67.4	1.8	265	11	236	8	−10	52	249	8
FL7-15.1	2632	4294	89.8	1.69	253	9	238	7	116	40	242	7
FL7-16.1	1077	1374	38.8	1.32	260	9	231	10	−79	99	277	8
FL7-17.1	495	2393	17.7	4.99	385	32	256	14	221	130	215	7
FL7-18.1	560	713	19.7	1.32	256	10	312	50	774	380	245	15
FL7-19.1	3609	9262	126	2.65	265	12	256	7	245	19	243	7
FL7-20.1	1718	3188	60.7	1.92	262	10	263	7	290	27	255	7
FL7-21.1	2127	3244	71.5	1.58	250	9	246	7	235	29	241	7
FL7-22.1	3303	8591	109	2.69	251	12	244	7	257	29	230	7
Sample FL44 (a diorite from the Anding intrusion)												
FL44-1	15953	13099	857	0.82	300	5	294	4	252	9	303	5
FL44-2	336	75	38	0.22	704	11	714	12	747	32	905	26
FL44-3	6580	16270	441	2.47	263	4	261	5	247	22	271	5
FL44-4	258	122	48	0.47	1049	17	1037	16	1014	30	1013	23
FL44-5	141	113	70	0.80	2247	32	2348	17	2438	12	2202	42
FL44-6	5455	15912	377	2.92	256	4	255	4	245	14	258	4
FL44-7	1682	3133	94	1.86	248	4	245	5	222	38	248	4
FL44-8	4970	6470	251	1.30	254	4	250	4	222	22	246	4
FL44-9	5701	12570	351	2.21	258	4	255	4	228	16	259	4
FL44-10	124	92	10	0.74	435	8	400	25	198	160	402	18
FL44-11	789	61	144	0.08	1155	18	974	13	585	24	910	32
FL44-12	6271	14745	393	2.35	255	4	252	4	224	21	252	4
FL44-13	9416	21483	604	2.28	268	4	264	4	230	12	262	4
FL44-14	13208	11381	659	0.86	278	4	274	4	236	9	272	4
FL44-15	5685	8157	291	1.43	253	4	251	4	229	14	243	4
FL44-16	7279	12413	401	1.71	257	4	257	4	261	12	249	4
FL44-17	138	87	2	0.63	100	2	105	5	219	94	108	4

Table 2 Major oxides and trace elements of the mafic rocks in Funing, SW China

Intrusion	Shadou sill (High-Ti group)											Yapai dyke (High-Ti group)			
Samples	FL-3	FL-4	FL-5	FL-6	FL-7	FL-8	FL-9	FL-10	FL-11A	FL-12	FL-13	FL-14	FL-15	FL-17	FL-18
Major oxides (wt%)															
SiO_2	47.6	45.4	45.3	45.8	45.5	45.5	45.3	45.6	45.4	45.6	45.7	47.8	45.2	45.5	46.3
TiO_2	2.87	3.03	3.07	2.00	3.65	3.11	3.09	2.30	1.55	1.81	2.90	2.87	4.44	1.75	2.35
Al_2O_3	13.59	13.72	14.29	15.29	12.53	13.65	13.67	15.01	11.88	12.49	14.27	13.63	14.97	14.14	17.52
$Fe_2O_3^a$	14.18	15.33	13.82	13.28	15.53	15.17	15.19	13.71	15.49	14.92	14.94	14.10	13.60	13.47	11.50
MnO	0.24	0.26	0.24	0.23	0.27	0.24	0.25	0.23	0.28	0.26	0.25	0.23	0.21	0.24	0.20
MgO	5.43	5.47	5.57	7.42	4.72	5.65	5.58	6.97	11.78	10.34	5.93	5.38	3.74	8.92	4.13
CaO	9.47	9.94	9.81	10.60	10.33	10.35	9.97	10.40	10.98	11.06	10.04	9.70	10.17	10.72	11.17
Na_2O	2.16	2.60	2.32	2.51	2.66	2.64	2.63	2.53	1.78	1.98	2.67	2.44	2.98	2.35	3.19
K_2O	1.19	1.25	1.49	0.76	1.27	1.13	1.17	0.88	0.46	0.59	1.09	1.06	1.17	0.73	0.82
P_2O_5	0.45	0.57	0.56	0.35	0.61	0.53	0.57	0.42	0.23	0.29	0.54	0.46	0.49	0.27	0.37
LOI	1.38	1.20	2.61	1.03	1.62	0.72	1.33	1.14	0.00	0.19	0.65	1.48	1.81	0.93	1.17
Sum	98.6	98.8	99.0	99.2	98.7	98.7	98.8	99.2	99.8	99.5	98.9	99.1	98.7	99.1	98.7
Trace elements (ppm)															
Sc	35.1	39.6	32.6	20.2	32.5	27.0	29.2	24.6	25.2	30.1	26.0	30.7	28.2	27.4	24.7
V	307	329	326	265	430	371	347	262	272	286	319	302	417	292	386
Cr	125	71.9	83.2	135	154	110	99.8	116	264	295	80.2	117	6.62	197	49.4
Ni	98	95	111	132	61.8	94.0	101	122	202	173	106	93.0	40.0	150	56.7
Cu	102	109	102	62.8	98.7	99.5	113	77.4	53.0	60.3	98.1	101	71.6	50.0	73.1
Rb	43.6	28.8	37.0	14.2	25.4	24.2	27.1	17.6	8.1	11.3	23.5	34.6	24.6	11.9	12.1
Sr	375	577	649	587	474	536	558	555	435	455	565	366	619	561	676
Y	35.2	27.8	28.2	17.9	33.6	27.4	27.7	21.0	13.7	16.3	26.0	34.9	25.9	15.4	18.8
Zr	186	143	141	88.4	205	151	140	106	60.1	73.2	135	180	139	74.1	93.3
Nb	27.0	24.3	24.7	14.9	29.5	23.7	24.4	18.1	9.48	11.7	23.1	26.3	24.6	11.7	15.7
Ba	333	607	878	414	726	560	623	474	273	332	562	287	601	384	452
La	29.9	30.3	30.9	19.5	35.0	29.2	30.6	22.8	12.5	16.0	28.4	29.1	28.0	15.8	20.3
Ce	64.1	65.3	66.4	41.9	76.3	63.2	66.1	49.3	27.7	35.0	61.4	62.9	61.0	34.4	43.7
Pr	8.27	8.51	8.78	5.49	10.0	8.31	8.57	6.48	3.68	4.63	8.07	8.12	7.93	4.53	5.78
Nd	35.7	37.8	38.6	24.6	44.4	37.1	38.3	28.5	16.9	20.8	35.7	35.6	34.8	20.3	25.3
Sm	7.67	7.58	7.78	4.88	9.04	7.46	7.62	5.71	3.60	4.41	7.27	7.61	7.03	4.18	5.13
Eu	2.43	2.87	2.89	2.04	3.14	2.75	2.89	2.22	1.50	1.76	2.64	2.30	2.78	1.90	2.20
Gd	7.04	6.44	6.58	4.26	7.62	6.32	6.57	4.94	3.20	3.83	6.13	6.83	5.98	3.64	4.44
Tb	1.18	1.01	1.01	0.67	1.21	0.98	1.01	0.76	0.51	0.60	0.94	1.15	0.94	0.55	0.69
Dy	6.53	5.36	5.45	3.53	6.48	5.30	5.29	4.05	2.69	3.19	4.98	6.45	5.03	3.03	3.59
Ho	1.37	1.09	1.11	0.71	1.33	1.06	1.10	0.84	0.55	0.65	1.03	1.35	1.02	0.62	0.75
Er	3.56	2.78	2.84	1.82	3.41	2.74	2.82	2.15	1.34	1.63	2.64	3.52	2.61	1.53	1.87
Tm	0.47	0.36	0.36	0.24	0.43	0.35	0.35	0.28	0.17	0.21	0.34	0.47	0.34	0.20	0.24
Yb	3.07	2.24	2.26	1.46	2.77	2.21	2.21	1.66	1.09	1.33	2.10	3.00	2.11	1.21	1.48
Lu	0.46	0.33	0.34	0.22	0.42	0.33	0.33	0.25	0.17	0.20	0.31	0.45	0.32	0.18	0.23
Hf	5.15	3.99	4.00	2.55	5.51	4.09	3.86	2.95	1.74	2.08	3.68	5.05	3.88	2.09	2.60
Ta	1.65	1.49	1.52	0.92	1.87	1.46	1.50	1.11	0.59	0.72	1.41	1.63	1.54	0.70	0.93
Pb	7.07	6.64	4.33	3.63	3.35	5.60	5.08	6.43	3.10	2.32	4.97	3.98	3.56	40.62	3.14
Th	3.99	2.93	2.98	1.79	4.01	2.79	2.77	2.06	1.08	1.38	2.68	3.86	2.62	1.42	1.77
U	1.11	0.77	0.85	0.51	1.16	0.81	0.76	0.69	0.33	0.40	0.76	1.06	0.74	0.40	0.51
Mg#	0.60	0.59	0.61	0.69	0.55	0.60	0.59	0.67	0.75	0.73	0.61	0.60	0.52	0.72	0.59

Intrusion	Yapai dyke (High-Ti group)							Anding dyke (High-Ti group)						
Sample	FL-19	FL-20	FL-21	FL-22	FL-26	FL-27	FL-28	FL-38	FL-47	FL-50	FL-51	FL-53	FL-54	FL-55A
Major oxides (wt%)														
SiO_2	44.2	46.1	45.4	47.9	46.1	46.6	45.7	46.9	44.8	46.3	45.2	44.5	45.4	44.6
TiO_2	1.77	3.95	3.10	2.84	3.08	2.71	3.07	2.69	3.70	3.33	4.34	4.21	2.98	3.12
Al_2O_3	13.60	13.42	13.78	13.61	17.20	18.04	17.21	12.62	14.20	16.38	13.46	13.56	13.99	13.29
Fe_2O_3	16.53	15.41	15.07	13.05	12.26	11.38	11.97	16.94	15.46	12.92	16.35	16.38	14.00	14.97
MnO	0.28	0.26	0.25	0.22	0.20	0.20	0.19	0.26	0.23	0.20	0.26	0.27	0.23	0.24
MgO	10.83	3.34	5.45	5.31	3.71	3.06	3.50	2.98	4.07	3.16	4.00	3.55	5.70	5.68
CaO	8.72	9.09	10.15	10.35	11.20	10.52	11.34	7.97	9.79	9.25	9.36	8.64	9.06	9.42
Na_2O	2.14	3.31	2.56	2.54	2.95	3.23	2.92	3.37	3.02	3.32	3.07	3.16	2.81	2.82
K_2O	0.62	1.48	1.18	0.68	0.94	1.03	0.90	1.73	1.28	1.49	1.47	1.53	1.34	1.42
P_2O_5	0.31	0.70	0.56	0.44	0.31	0.40	0.31	1.00	0.53	0.56	0.62	0.68	0.52	0.58
LOI	0.09	1.69	1.55	1.71	1.66	1.82	2.20	2.35	1.86	1.99	1.03	2.32	2.88	2.98
Sum	99.0	98.7	99.0	98.7	99.6	99.0	99.4	98.8	98.9	98.9	99.2	98.8	98.9	99.1

Table 2 Contd.

Intrusion	Yapai dyke (High-Ti group)							Anding dyke (High-Ti group)						
Sample	FL-19	FL-20	FL-21	FL-22	FL-26	FL-27	FL-28	FL-38	FL-47	FL-50	FL-51	FL-53	FL-54	FL-55A
Trace elements (ppm)														
Sc	16.1	27.1	36.0	26.3	22.8	18.7	31.1	20.4	34.4	25.2	34.3	24.0	27.4	24.4
V	190	316	343	318	627	496	584	166	577	411	400	412	328	333
Cr	86.5	20.8	86.8	125	75.5	47.9	51.8	26.5	58.6	18.3	51.5	26.9	97.7	66.4
Ni	224	44.8	93.0	52.6	45.7	46.5	41.7	71.2	59.4	36.8	58.9	59.3	85.1	98.7
Cu	67.8	114	102	73.9	59.1	75.5	62.1	193	85.5	91.9	113	116	64.7	95.6
Rb	11.6	36.4	25.9	26.7	14.8	16.6	13.8	46.0	28.3	29.3	29.6	32.1	32.4	31.4
Sr	510	571	566	346	705	716	786	501	634	706	595	632	620	710
Y	15.8	36.0	27.1	35.7	17.9	20.0	18.1	46.0	27.1	27.6	31.2	33.6	25.7	27.8
Zr	81.5	207	142	188	89.0	102	94.8	236	133	147	163	177	133	138
Nb	13.9	31.7	24.0	26.5	15.0	16.6	16.2	33.3	20.2	24.2	29.6	31.2	22.6	23.9
Ba	747	679	570	246	526	490	538	856	688	920	764	814	706	806
La	17.1	41.6	29.2	29.7	18.4	21.9	19.1	52.1	30.0	31.1	35.2	37.0	27.6	30.1
Ce	37.1	88.8	63.1	63.7	39.9	47.2	41.2	112	64.1	66.6	75.5	80.1	59.9	65.1
Pr	4.82	11.53	8.22	8.20	5.24	6.08	5.44	14.55	8.31	8.66	9.79	10.42	7.86	8.44
Nd	21.4	49.8	36.6	35.4	23.4	27.1	24.1	63.9	36.5	38.1	42.8	45.9	34.5	37.8
Sm	4.21	9.90	7.45	7.46	4.74	5.38	4.92	12.41	7.35	7.51	8.47	9.12	6.82	7.47
Eu	1.72	3.59	2.79	2.39	2.11	2.30	2.16	4.11	2.85	2.86	3.24	3.24	2.57	2.69
Gd	3.66	8.33	6.25	6.92	4.12	4.61	4.18	10.52	6.27	6.49	7.20	7.74	5.94	6.39
Tb	0.58	1.28	0.97	1.15	0.65	0.71	0.66	1.63	0.98	1.00	1.10	1.18	0.92	0.99
Dy	3.06	6.86	5.17	6.54	3.37	3.80	3.49	8.58	5.17	5.17	5.97	6.29	4.81	5.23
Ho	0.62	1.40	1.05	1.35	0.71	0.78	0.70	1.75	1.07	1.07	1.22	1.28	0.99	1.08
Er	1.61	3.59	2.67	3.51	1.80	1.96	1.83	4.46	2.70	2.70	3.02	3.35	2.54	2.70
Tm	0.20	0.45	0.35	0.47	0.23	0.25	0.23	0.59	0.35	0.34	0.40	0.42	0.32	0.34
Yb	1.30	2.86	2.12	2.98	1.45	1.62	1.49	3.68	2.18	2.18	2.53	2.67	2.01	2.14
Lu	0.20	0.43	0.32	0.45	0.22	0.24	0.23	0.54	0.32	0.33	0.38	0.41	0.31	0.32
Hf	2.20	5.49	3.83	5.08	2.49	2.74	2.58	6.00	3.71	3.92	4.32	4.69	3.62	3.73
Ta	0.84	1.94	1.43	1.62	0.90	1.01	0.97	1.99	1.21	1.44	1.79	1.86	1.34	1.43
Pb	14.95	7.03	4.87	5.68	3.24	3.70	3.21	16.40	3.88	3.38	3.78	3.97	2.85	3.59
Th	1.54	3.76	2.78	4.00	1.67	2.09	1.75	4.77	3.08	2.98	3.24	3.60	2.57	2.70
U	0.44	0.98	0.80	1.13	0.48	0.60	0.50	1.28	0.81	0.84	0.88	1.03	0.71	0.71
Mg#	0.72	0.46	0.59	0.62	0.55	0.52	0.54	0.41	0.51	0.49	0.49	0.46	0.62	0.60

Intrusion	Yapai intrusion (Low-Ti group)								Anding intrusion (Low-Ti group)					
Sample	FL-16	FL-23	FL-24	FL-25	FL-29	FL-30	FL-31	FL-32	FL-33	FL-34	FL-35	FL-36	FL-37	FL-39
Major oxides (wt%)														
SiO_2	50.5	51.5	52.0	51.5	51.2	49.9	50.4	50.7	52.1	51.1	51.5	45.5	46.8	51.1
TiO_2	0.58	0.69	0.64	0.73	0.63	0.56	0.56	0.56	0.54	0.50	0.57	0.59	0.60	0.56
Al_2O_3	14.57	14.86	14.60	14.56	11.63	13.10	13.05	11.82	12.22	11.55	13.41	13.83	11.98	12.99
Fe_2O_3	8.48	8.60	8.44	8.92	9.02	8.75	8.66	8.90	8.86	10.37	8.99	10.43	10.84	9.15
MnO	0.15	0.17	0.16	0.16	0.18	0.17	0.17	0.17	0.19	0.19	0.20	0.19	0.19	0.19
MgO	8.85	7.40	7.38	7.69	11.11	10.34	9.92	11.31	11.02	12.53	10.92	14.92	14.22	11.55
CaO	8.68	8.22	9.29	8.40	10.18	10.34	10.32	10.80	10.77	9.13	9.48	8.83	10.39	9.35
Na_2O	1.68	1.84	1.78	2.00	1.40	1.39	1.33	1.22	1.20	1.26	1.49	1.63	1.19	1.55
K_2O	1.53	2.06	1.63	1.95	1.31	0.69	0.68	0.93	0.91	0.90	1.15	0.47	0.64	0.91
P_2O_5	0.06	0.07	0.05	0.08	0.06	0.06	0.05	0.06	0.06	0.06	0.06	0.06	0.06	0.06
LOI	3.74	3.25	3.30	3.17	2.62	3.95	3.86	2.64	1.54	1.25	1.68	2.23	2.36	1.54
Sum	98.8	98.7	99.2	99.1	99.3	99.2	99.0	99.1	99.4	98.9	99.4	98.7	99.3	99.0
Trace elements (ppm)														
Sc	24.0	21.5	30.4	26.5	35.0	31.7	36.7	31.4	28.8	26.5	23.1	16.0	31.1	23.2
V	181	179	179	185	206	200	201	199	195	173	169	128	157	163
Cr	543	350	354	331	740	804	750	814	755	1168	1028	591	899	1037
Ni	96.6	61.8	56.8	67.7	140	132	126	127	183	926	179	529	337	211
Cu	44.2	41.6	37.1	41.7	57.3	61.4	54.8	51.8	97.1	457	62.3	143	76.2	59.3
Rb	72.2	85.2	66.7	83.2	60.2	30.0	31.0	42.5	45.5	44.3	51.8	18.4	26.9	42.1
Sr	130	133	177	135	102	122	129	106	87.3	83.9	103	116	97.5	89.1
Y	23.4	26.6	24.7	26.7	22.5	21.0	21.3	20.5	21.4	18.9	19.1	16.2	18.3	18.8
Zr	81.0	100	92.8	96.4	62.6	66.8	68.9	65.6	71.0	63.9	67.9	50.5	50.4	72.7
Nb	4.10	5.05	4.54	5.33	3.45	3.44	3.34	3.24	3.59	3.28	3.65	2.42	2.46	3.83
Ba	248	325	269	308	204	123	120	179	151	130	165	88.1	91.4	142
La	13.0	15.1	14.0	14.7	9.78	10.1	10.3	13.9	10.9	9.32	9.81	6.51	6.64	10.0
Ce	25.8	30.0	27.5	29.6	20.1	20.3	20.5	22.5	21.9	18.6	19.5	13.2	13.7	20.0
Pr	3.20	3.60	3.34	3.61	2.57	2.52	2.56	2.54	2.68	2.26	2.40	1.70	1.78	2.44
Nd	13.0	15.0	13.7	15.1	11.3	10.7	10.8	10.4	11.1	9.65	10.0	7.40	7.94	10.0

Table 2 Contd.

Sm	3.08	3.63	3.19	3.56	2.84	2.57	2.60	2.50	2.67	2.27	2.38	1.94	2.07	2.40
Eu	0.74	0.85	0.84	0.95	0.67	0.75	0.74	0.70	0.67	0.58	0.66	0.73	0.67	0.64
Gd	3.21	3.61	3.31	3.67	2.89	2.78	2.81	2.62	2.88	2.42	2.48	2.11	2.29	2.43
Tb	0.60	0.68	0.62	0.71	0.56	0.54	0.53	0.51	0.54	0.47	0.47	0.42	0.45	0.47
Dy	3.84	4.31	3.98	4.35	3.59	3.36	3.42	3.25	3.46	3.03	3.01	2.60	2.90	3.02
Ho	0.88	0.99	0.92	0.99	0.84	0.78	0.79	0.76	0.79	0.69	0.70	0.59	0.67	0.69
Er	2.51	2.83	2.60	2.81	2.33	2.19	2.21	2.17	2.24	2.02	2.00	1.66	1.94	1.95
Tm	0.36	0.40	0.38	0.39	0.33	0.32	0.33	0.31	0.32	0.29	0.29	0.24	0.28	0.29
Yb	2.39	2.67	2.48	2.66	2.24	2.10	2.12	2.06	2.14	1.92	1.89	1.57	1.80	1.89
Lu	0.37	0.40	0.38	0.41	0.35	0.33	0.33	0.32	0.34	0.30	0.30	0.24	0.28	0.29
Hf	2.43	2.92	2.72	2.81	1.92	1.97	2.03	1.90	2.08	1.89	1.93	1.47	1.51	2.09
Ta	0.31	0.38	0.35	0.39	0.25	0.25	0.26	0.24	0.26	0.25	0.27	0.17	0.19	0.28
Pb	4.13	13.88	7.84	9.23	10.48	4.23	10.79	4.92	9.91	9.73	7.24	5.12	5.44	6.57
Th	4.97	6.02	5.45	5.79	3.44	3.80	3.94	3.70	4.13	3.50	3.63	1.94	2.28	3.74
U	1.21	1.54	1.38	1.43	0.89	0.97	1.01	1.13	1.03	0.86	0.93	0.51	0.59	0.95
Mg#	0.81	0.77	0.78	0.77	0.83	0.82	0.82	0.83	0.83	0.83	0.83	0.85	0.84	0.83

Intrusion	Anding intrusion (Low-Ti group)										Basalts (Low-Ti group)				
Sample	FL-40	FL-41	FL-42	FL-43	FL-44	FL-45	FL-46	FL-48	FL-49	FL-52	FL-55	FL-56	FL-57	FL-58	FL-59
Major oxides (wt%)															
SiO_2	44.3	51.0	44.0	45.4	51.5	51.0	57.5	51.5	52.2	47.5	58.3	51.5	56.8	54.5	57.8
TiO_2	0.52	0.54	0.54	0.65	0.56	0.57	1.19	0.69	0.78	0.60	1.01	1.05	1.12	1.05	0.94
Al_2O_3	8.78	12.45	10.93	12.44	13.37	12.64	13.52	13.90	15.33	13.27	12.52	14.72	13.60	14.14	13.42
Fe_2O_3	14.28	9.41	12.83	11.78	9.03	8.90	10.53	9.15	8.81	9.05	9.29	10.44	9.02	9.81	8.85
MnO	0.22	0.19	0.22	0.21	0.17	0.17	0.18	0.17	0.17	0.17	0.14	0.18	0.16	0.18	0.17
MgO	19.62	12.01	18.69	15.71	10.12	10.08	3.22	7.93	6.65	11.63	5.23	6.16	4.46	5.27	4.59
CaO	7.87	9.29	7.40	8.71	10.54	10.97	5.70	9.36	9.79	10.46	5.75	7.85	5.13	6.21	6.64
Na_2O	0.96	1.34	1.04	1.30	1.49	1.84	2.33	1.79	1.84	2.10	2.10	2.98	2.13	1.81	1.60
K_2O	0.35	0.80	0.66	0.57	0.75	0.78	2.89	1.37	1.67	0.72	0.92	1.23	3.37	1.92	2.46
P_2O_5	0.05	0.05	0.06	0.07	0.07	0.07	0.14	0.07	0.10	0.05	0.14	0.12	0.16	0.14	0.13
LOI	1.53	1.80	2.57	2.24	1.88	1.80	2.03	3.12	1.61	3.69	3.57	3.23	2.65	3.73	2.46
Sum	98.5	98.9	98.9	99.1	99.5	98.8	99.3	99.1	99.0	99.2	98.9	99.4	98.5	98.8	99.0
Trace elements (ppm)															
Sc	30.2	21.9	25.1	19.0	26.6	30.2	24.9	27.4	22.0	28.0	32.1	30.5	25.9	31.0	25.2
V	142	170	129	140	174	186	170	183	172	177	166	213	181	173	161
Cr	781	1095	494	471	691	754	9.23	469	361	981	251	188	198	233	198
Ni	1380	264	747	524	273	408	0.48	66.4	45.2	270	49.4	52.4	42.9	50.9	35.8
Cu	568	89.7	183	117	216	189	21.7	37.1	38.7	65.5	23.3	40.1	33.4	32.4	28.1
Rb	17.3	38.6	26.9	23.8	34.3	40.0	130	59.7	79.8	21.8	27.0	87.8	115	108	106
Sr	73.0	84.1	102	105	103	95.4	167	154	148	128	97.5	242	219	256	155
Y	15.2	18.4	15.3	17.5	21.2	21.9	50.7	27.2	27.5	19.0	44.4	34.8	44.1	46.3	42.3
Zr	42.6	61.8	45.1	53.4	71.3	73.1	202	88.9	106	50.4	199	125	193	198	190
Nb	2.08	3.25	2.23	2.59	3.53	3.69	10.6	4.97	5.85	2.39	10.4	6.48	11.1	10.6	9.83
Ba	67.8	116	79.8	87.5	141	177	448	228	274	237	172	217	799	398	393
La	5.46	8.78	5.55	6.72	10.9	11.2	32.6	14.4	16.5	6.78	30.7	17.5	31.2	31.1	29.8
Ce	11.3	17.6	11.5	13.9	21.9	22.7	63.5	29.0	32.8	14.1	61.0	35.2	61.6	61.8	58.1
Pr	1.44	2.18	1.49	1.78	2.68	2.83	7.65	3.59	3.98	1.81	7.43	4.32	7.43	7.45	7.03
Nd	6.37	9.18	6.59	7.94	11.2	11.6	31.1	14.8	16.7	8.16	29.9	17.9	30.5	30.0	28.2
Sm	1.72	2.19	1.80	2.09	2.66	2.81	7.12	3.51	3.86	2.14	6.55	4.35	6.66	6.77	6.20
Eu	0.56	0.60	0.57	0.66	0.69	0.66	1.41	0.80	1.00	0.70	1.00	1.09	1.35	1.13	1.22
Gd	1.86	2.32	1.95	2.19	2.80	2.94	6.98	3.64	3.80	2.36	6.40	4.55	6.53	6.63	6.17
Tb	0.37	0.44	0.38	0.44	0.53	0.55	1.29	0.69	0.72	0.47	1.16	0.87	1.17	1.21	1.13
Dy	2.46	2.85	2.44	2.78	3.39	3.54	7.91	4.37	4.43	3.03	7.10	5.59	7.09	7.40	6.87
Ho	0.57	0.68	0.57	0.65	0.78	0.80	1.81	1.00	1.01	0.70	1.62	1.29	1.59	1.68	1.55
Er	1.58	1.89	1.64	1.81	2.22	2.28	5.08	2.78	2.82	1.97	4.50	3.66	4.47	4.73	4.30
Tm	0.23	0.28	0.23	0.26	0.32	0.32	0.73	0.41	0.41	0.28	0.63	0.53	0.64	0.67	0.62
Yb	1.52	1.87	1.52	1.73	2.10	2.11	4.76	2.66	2.69	1.86	4.22	3.51	4.20	4.41	4.11
Lu	0.24	0.29	0.24	0.27	0.33	0.33	0.72	0.41	0.42	0.29	0.66	0.54	0.64	0.68	0.63
Hf	1.26	1.78	1.31	1.55	2.11	2.14	5.78	2.60	3.05	1.50	5.75	3.58	5.47	5.65	5.33
Ta	0.15	0.24	0.16	0.19	0.27	0.28	0.78	0.38	0.42	0.18	0.77	0.47	0.82	0.79	0.72
Pb	8.20	7.70	4.22	5.52	13.62	11.24	15.23	5.17	11.31	3.56	6.33	3.32	15.77	20.36	17.29
Th	1.82	3.19	1.72	2.10	4.07	4.26	12.62	5.31	6.30	2.20	13.04	6.54	12.14	12.76	12.34
U	0.48	0.82	0.46	0.57	1.06	1.03	3.13	1.25	1.54	0.59	3.19	1.63	2.96	3.12	2.99
Mg#	0.84	0.83	0.85	0.84	0.82	0.82	0.55	0.77	0.75	0.84	0.69	0.70	0.66	0.68	0.67

LOI = loss on ignition

[a]Fe_2O_3 as total Fe

in concentrations greater than 0.5 wt% and ± 5% (relative) for minor oxides present in concentrations greater than 0.1%. The accuracies of the ICP-MS analyses are estimated to be better than ± 5% (relative) for most elements.

Rb–Sr and Sm–Nd isotopic analyses

Isotope ratios of Sr–Nd and concentrations of Rb, Sr, Sm, and Nd were determined on a VG-354 thermal ionization magnetic sector mass spectrometer at the Institute of Geology and Geophysics, Chinese Academy of Sciences, Beijing. The chemical separation and isotopic measurement procedures are described in Zhang et al. (2001). Mass fractionation corrections for Sr and Nd isotopic ratios were based on values of $^{86}Sr/^{88}Sr$ = 0.1194 and $^{146}Nd/^{144}Nd$ = 0.7219. Uncertainties in Rb/Sr and Sm/Nd ratios are less than ± 2% and ± 0.5% (relative), respectively.

Analytical results

SHRIMP zircon analytical results

Two samples were selected for zircon separation. Sample FL7 is a diabase from the Shadou sill and belongs to the high-Ti group (Table 2). Sample, FL44, is a diorite from the Anding intrusion and is of the low-Ti group (Table 2).

Zircon grains from sample FL7 of the Shadou sill exhibit a variety of textures and morphologies characteristic of magmatic origin. Twenty analyses were obtained using the Beijing SHRIMP II (Table 1). Except for one analysis that yielded an older age of around 310 Ma, all analyses, including those of cores, rims, high- and low-U zones, and crystals of different shapes, gave a single age. One analysis has a large error and is omitted from the mean. The remaining 18 analyses yielded a mean $^{206}Pb/^{238}U$ age of 260 ± 3 Ma (Fig. 2; all uncertainties are 2σ). All 18 grains are from a single-age population of zircons, and there is no evidence of any disturbance since 260 Ma. The observed complex zonation of the zircons in FL7 most likely occurred during cooling and crystallization of the diorite. The 260-Ma age of the zircons from sample FL7 is therefore considered to be the best estimate of the crystallization age for the Shadou sill.

Numerous igneous zircon grains were separated from diorite FL44 of the Anding intrusion. Sixteen analyses were obtained using the Perth SHRIMPII. Six xenolithic zircon grains were identified and these have $^{206}Pb/^{238}U$ ages ranging from 300 Ma to 2247 (Table 1). A group of eight analyses yielded a mean $^{206}Pb/^{238}U$ age of 258 ± 3 Ma (Fig. 2). Thus, 258 Ma is the best estimate of the crystallization age of the Anding intrusion, slightly younger than the age of the Shadou sill (sample FL7) (Fig. 2).

Whole-rock geochemical data

The mafic rocks in Funing have a wide range of chemical compositions (Table 2). Both the undifferentiated sills and layered intrusions display variable geochemical features. The volcanic rocks have similar compositions to the upper part of the layered intrusions.

The sills have highly variable TiO_2 (1.55–4.44 wt%), much higher than that of the layered intrusions and volcanic rocks (< 1.19 wt% TiO_2). The former is termed as the high-Ti group and the latter as the low-Ti group (Table 2). The high-Ti group has a narrow range of SiO_2 (44.2–47.9 wt%), whereas the low-Ti group has variable SiO_2 ranging from 44.0 to 58.3 wt% (Table 2). The high-Ti group is also enriched in Al_2O_3, Fe_2O_3, and P_2O_5 relative to the low-Ti group. The two groups show markedly different trends in the plots of SiO_2 versus oxides and MgO versus Fe_2O_3 and TiO_2 (Fig. 3a-f). For the high-Ti group, there is a clear negative correlation between MgO and TiO_2 (Fig. 3f). Although both the high- and low-Ti groups plot in distinct fields in the AFM diagram, they both have tholeiitic trends (Fig. 4).

In general, Ni has a positive correlation with MgO, whereas Cu does not correlate significantly with MgO (Fig. 5a, b). In the plots of Cu versus Ni, there is a very good positive correlation for samples from the low-Ti group (Fig. 5c). Overall, the high-Ti group has much more variable Cu/Ni ratios than the low-Ti group (Fig. 5d). The low-Ti group has a much wider range of Ni/MgO ratios than the high-Ti group (Fig. 5e). The high-Ti group has higher but variable V contents and Ti/V ratios than the low-Ti group (Fig. 5e, f).

The two groups also have different REE and trace element patterns. The high-Ti group has (La/Yb)cn (chondrite normalized) ratios between 6.99 and 10.45, exhibits LREE enrichment, and has positive Eu anomalies (Fig. 6a), whereas the low-Ti group has (La/Yb)cn ratios between 2.58 and 5.33, has relatively flat chondrite-normalized REE patterns, and exhibits negative Eu anomalies (Fig. 6b). The volcanic rocks have the same REE patterns as the other low-Ti rocks but their REE contents are somewhat higher. In primitive mantle-normalized spidergrams, the high-Ti group is characterized by enrichment in Ba relative to Rb and Th and especially in the Anding intrusion (except sample FL38) by marked negative Pb anomalies (Fig. 7a). Unlike the high-Ti group, the low-Ti rocks are characterized by negative Nb–Ta and Ti and P anomalies and positive Zr–Hf and Pb anomalies (Fig. 7b).

Nb and Yb are positively correlated but exhibit different trends for the high- and low-Ti groups (Fig. 8a). The two groups also have different ratios of Tb/Yb, Zr/

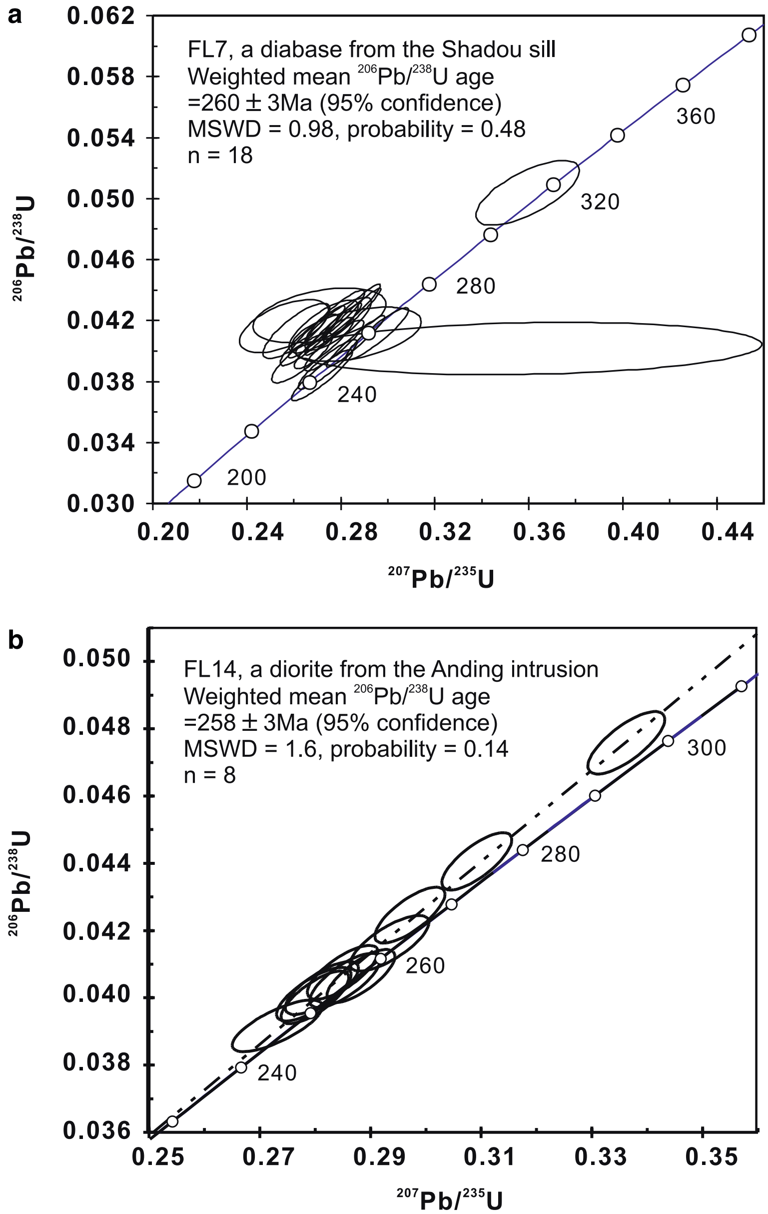

Fig. 2 SHRIMP zircon U–Pb concordia plots for samples FL7 (a diabase from the Shadou sill) (**a**) and FL44 (a diorite from the Anding intrusion) (**b**) from Funing, Yunnan, SW China (see Fig. 1 for locations of each intrusion)

Table 3 Rb-Sr and Sm-Nd isotopic analytical results of the mafic rocks in Funing, SW China

	Rb(ppm)	Sr(ppm)	$^{87}Rb/^{86}Sr$	$^{87}Sr/^{86}Sr_i$	2δ	Sm(ppm)	Nd(ppm)	$^{147}Sm/^{144}Nd$	$(^{143}Nd/^{144}Nd)_i$	2δ	εNd(t)
High-Ti group											
FL-5	34.4	640.77	0.155	0.706184	0.000016	7.30	34.27	0.1288	0.512591	0.000010	−0.9
FL-8	23.0	528.40	0.126	0.706025	0.000012	7.23	33.78	0.1294	0.512562	0.000009	−1.5
FL-12	10.4	452.54	0.066	0.706124	0.000020	4.19	18.94	0.1337	0.512606	0.000010	−0.6
FL-22	25.9	328.77	0.228	0.706780	0.000018	7.13	31.23	0.1380	0.512604	0.000013	−0.7
FL-38	42.0	491.03	0.248	0.706481	0.000020	11.99	57.39	0.1264	0.512574	0.000012	−1.2
FL-53	29.4	609.83	0.139	0.706284	0.000018	8.72	40.59	0.1299	0.512574	0.000010	−1.2
Low-Ti group											
FL-16	71.6	124.94	1.659	0.714578	0.000020	2.94	11.57	0.1538	0.512199	0.000009	−8.6
FL-30	28.5	120.02	0.687	0.712227	0.000020	2.56	9.77	0.1583	0.512265	0.000010	−7.3
FL-34	47.0	83.03	1.6390	0.715257	0.000018	2.22	8.46	0.1584	0.512247	0.000016	−7.6
FL-42	28.0	98.53	0.824	0.710289	0.000017	1.70	5.85	0.1763	0.512431	0.000008	−4.0
FL-48	52.7	149.02	1.025	0.712903	0.000020	3.43	13.47	0.1540	0.512204	0.000008	−8.5
FL-58	101.6	250.65	1.173	0.713723	0.000020	6.45	26.56	0.1468	0.512147	0.000009	−9.6

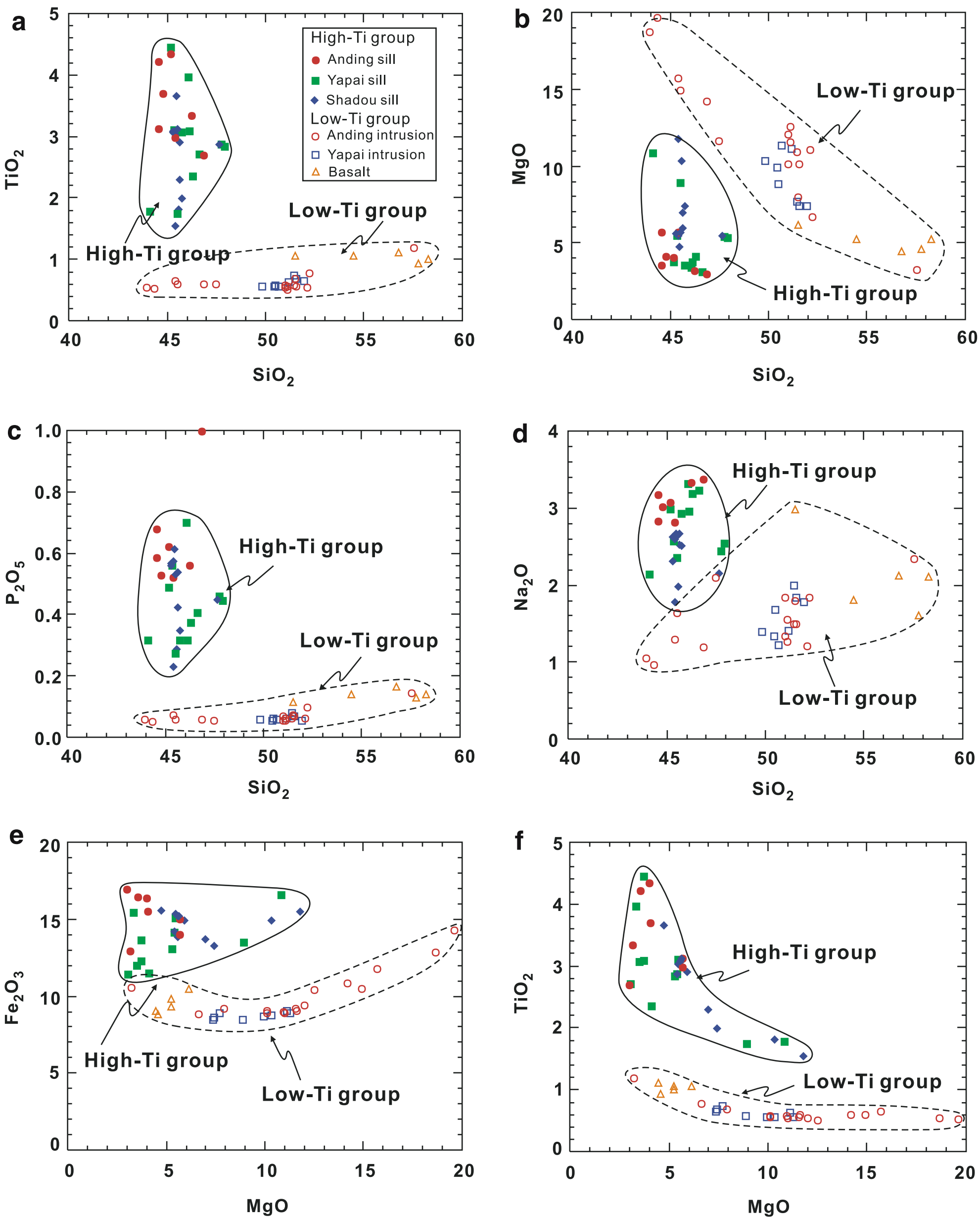

Fig. 3 Harker diagrams of major oxides of the mafic rocks in Funing, SW China: (**a**) SiO_2 versus TiO_2; (**b**) SiO_2 versus MgO; (**c**) SiO_2 versus P_2O_5; (**d**) SiO_2 versus Na_2O; (**e**) MgO versus $Fe_2O_{3(total)}$; and (**f**) MgO versus TiO_2

Y, Th/Yb, Ta/Yb, (Dy/Yb)cn and (La/Yb)cn, defining two different trends (Fig. 8b–d).

Rb–Sr and Sm–Nd isotopic compositions

Samples from Funing display large variations in the Rb–Sr and Sm–Nd isotopic compositions (Table 3). The low-Ti group has $(^{87}Sr/^{86}Sr)_i$ (initial) ratios ranging from 0.710 to 0.715, much more variable and higher than the high-Ti group (0.706–0.707) (Table 3). Although Rb–Sr isotopic variations can be partly due to the mobile nature of Rb and Sr during alteration (e.g., Rollison 1993), the large differences between the two groups of rocks reflect their different origins. On the other hand, the Sm–Nd isotopic compositions within the high and low-Ti groups are relatively constant. The initial εNd values range from −1.5 to −0.6 for the high-Ti group and from −9.6 to −4.0 for the low-Ti group. Both the εNd values and $(^{87}Sr/^{86}Sr)_i$ ratios show a good correlation with trace elemental ratios (Fig. 9a–d). There is a positive correlation between Th/Nb and $(^{87}Sr/^{86}Sr)_i$ ratios (Fig. 9a), but a negative correlation between Ce/Pb and $(^{87}Sr/^{86}Sr)_i$ ratio (Fig. 9b). The high-Ti group has lower Th/Nb and Rb/Nb but higher $(^{143}Nd/^{144}Nd)_i$ ratios than the low-Ti group (Fig. 9c, d).

All εNd values show an overall negative correlation with $(^{87}Sr/^{86}Sr)_i$ ratios (Fig. 10a). The high-Ti group plots in the field of the Emeishan flood basalts (Fig. 10a).

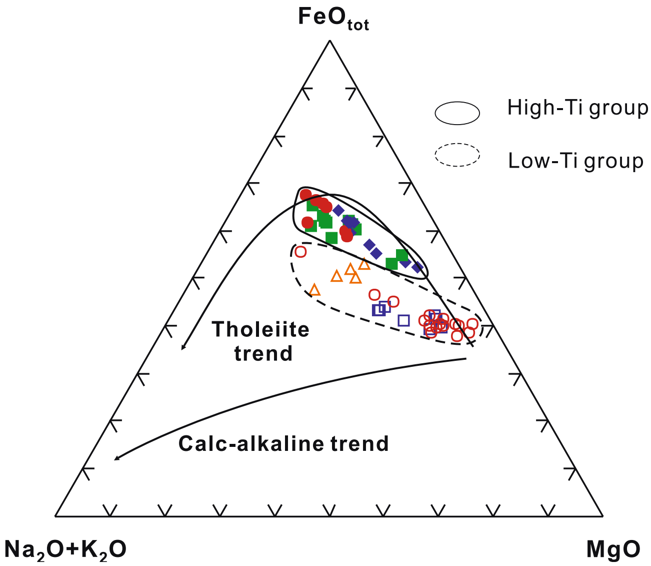

Fig. 4 Plots of AFM [($Na_2O + K_2O$)-FeOt-MgO] ternary diagram for the mafic rocks in Funing, SW China

Discussion

Petrogenesis of the Funing mafic rocks

The plutonic and volcanic mafic rocks in Funing form a widespread sub-volcanic and volcanic system (Fig. 1). The plutonic suite includes undifferentiated diabase sills and layered intrusions. Although geochemically the rocks belong to the high- and low-Ti groups, they have similar crystallization ages within the uncertainties (Fig. 2). The volcanic rocks are compositionally identical to the upper part of the layered intrusions. The close spatial and temporal association of the volcanic and plutonic rocks indicates that they formed from the same magmatic event. However, significant geochemical differences between the high- and low-Ti groups indicate that a variety of processes were involved in their formation, as invoked for LIPs elsewhere (Naldrett et al. 1992; Arndt et al. 1993, 1998, 2003; Lightfoot et al. 1990, 1993, 1994; Fedorenko and Czamanske 1997). Such processes include different degrees of fractional crystallization, different degrees of crustal contamination, and different mantle sources.

Fractional crystallization

Fractional crystallization (FC) appears to have played a major role in the compositional evolution of the Funing mafic rocks (Fig. 11). Compositional variations within the low and high-Ti groups can be easily explained by this process. For example, the negative Sr and Eu anomalies of the low-Ti group (Figs. 6 and 7) are likely to have resulted from plagioclase fractionation. The large variations of SiO_2 and MgO are also due to FC. The andesitic basalts are similar to the diorites in the layered intrusions, suggesting that they formed from an evolved magma that formed the upper portion of the layered intrusions.

The large variations of Cu and Ni with constant Cu/Ni ratios in the low-Ti group are controlled by the segregation of sulfide, because both Cu and Ni similarly prefer sulfide melts over silicate magmas (e.g., Naldrett 2004). The constant V and variable Ni/MgO ratios of the low-Ti group are a reflection of sulfide segregation without the involvement of magnetite. In the high-Ti group the large variations of TiO_2 and P_2O_5 are due to variable accumulation of magnetite and apatite. In contrast to the low-Ti group, sulfide is not an important phase in the high-Ti group and the variable Cu/Ni ratios in these rocks indicate mafic mineral fractionation/crystallization. TiO_2 and V are controlled mainly by magnetite. The large variation of V with constant Ni/MgO ratios in the high-Ti group (Fig. 5) is consistent with magnetite accumulation with no sulfide involvement. The positive Sr and Eu anomalies are probably due to accumulation of plagioclase.

Crustal contamination

The different trends of the low- and high-Ti groups in the Harker diagrams (Fig. 3) cannot be produced by FC of the same magma. The pronounced differences in some incompatible elements and their ratios between the high- and low-Ti groups suggest that they were derived from different magmas with different degrees of crustal contamination, because these elemental ratios are insensitive to alteration, melting conditions, and FC. Because of the relatively high $(^{87}Sr/^{86}Sr)_i$ and low εNd values of the low-Ti group, which contains abundant xenolithic zircon, contamination appears to have played an important role. The low-Ti group is much richer in some incompatible elements and is characterized by pronounced negative anomalies of Nb–Ta and Ti–P (Fig. 7). Because continental crust is poor in these elements (e.g., Rollison 1993), the distinctive negative anomalies (Fig. 7) can be accounted for by extensive crustal contamination.

The larger scatter of both $(^{87}Sr/^{86}Sr)_i$ and εNd values of the low-Ti group is consistent with variable degrees of crustal contamination (Fig. 10). Samples with high $(^{87}Sr/^{86}Sr)_i$ ratios and low εNd values have higher SiO_2 contents and Th/Nb ratios and lower TiO_2, clearly demonstrating an evolution involving assimilation and fractional crystallization (AFC) (Fig. 11).

In the plot of εNd versus $(^{87}Sr/^{86}Sr)_i$, the low-Ti group lies between the enriched mantle (EM2) and upper crust (UC), away from the "mantle array" (Fig. 10b). This requires a significant degree of crustal contamination either in the mantle source or during magma ascent and differentiation. Assuming that the crustal contamination occurred during emplacement of the magmas, modeled degrees of crustal contamination are high ($>$20%). Although crustal contamination would have

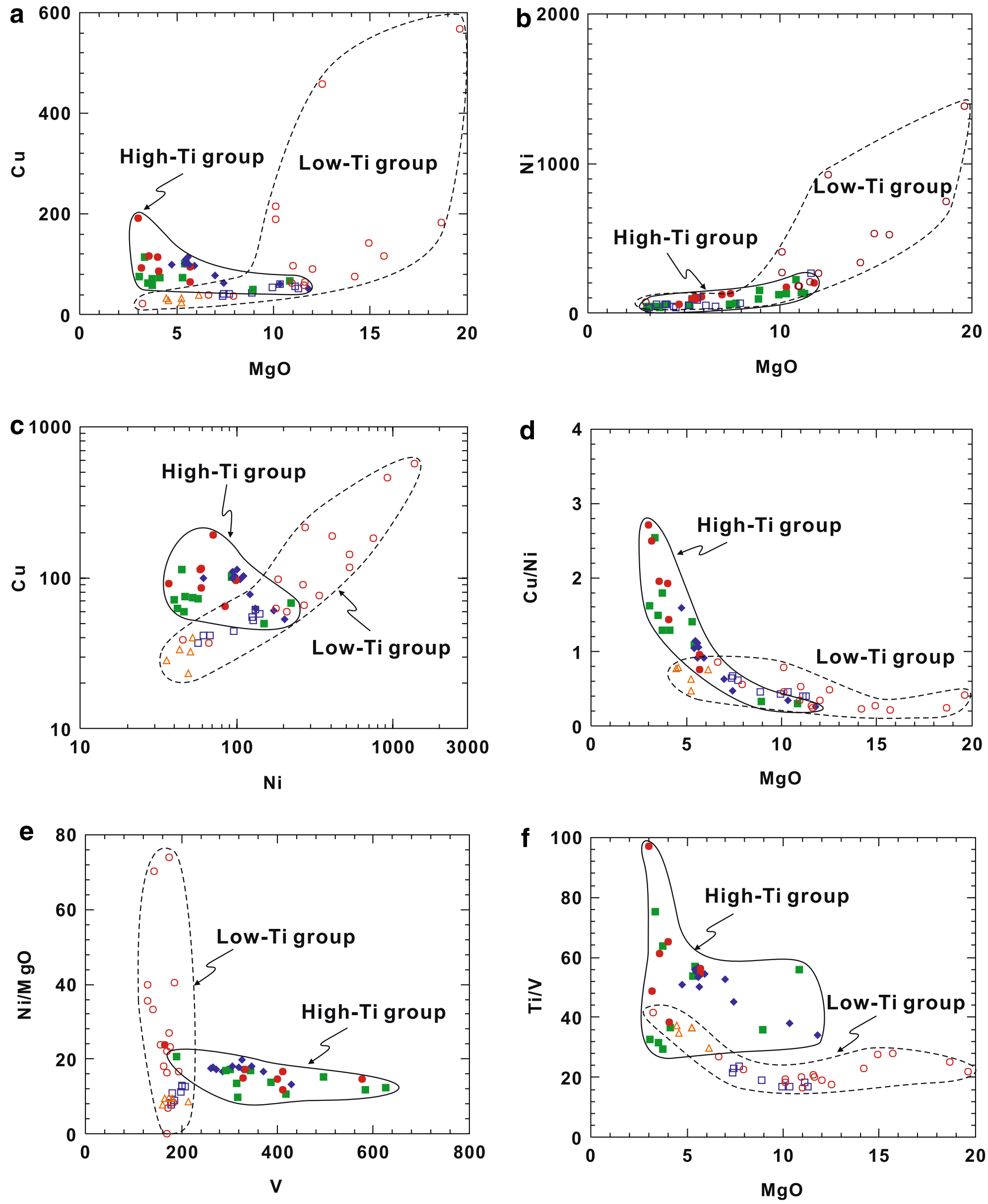

Fig. 5 Plots of the mafic rocks in Funing, SW China: **a** MgO versus Cu; **b** MgO versus Ni; **c** Cu versus Ni; **d** MgO versus Cu/Ni; **e** V versus Ni/MgO (ppm/wt%); and **f** MgO versus Ti/V

increased the rocks with ratios of LILE (large ion lithophile elements, such as Th, Rb, and Ba) and HFSE (high-field strength elements, such as Nb, Ta, Zr, and Hf), rocks of the low-Ti group have ratios of Th/Nb (>0.7) and Th/La (>0.3) even higher than the average upper continental crust (Fig. 12). A possible explanation is that it was derived from an enriched mantle source previously metasomatized by crustal fluids, such as fluids derived from altered rocks of oceanic crust with high Th/Nb ratios (~42) (Dorlendorf et al. 2000) (Fig. 12). There are two types of EM sources: EM1 and EM2. An EM2-type source has higher Th/La and Zr/Nb ratios than an EM1-type source. It is generally characterized by $(^{87}Sr/^{86}Sr)_i$ ratios (>0.7065) and intermediate $(^{143}Nd/^{144}Nd)_i$ ratios (Hart 1988; Weaver 1991). Therefore, the low-Ti group rocks have $(^{87}Sr/^{86}Sr)_i$ ratios and εNd values displaying an affinity to an EM2-like source.

We use average compositions of the lower and upper crusts in our modeling. Assuming an EM2-like parental magma, most of the low-Ti samples had 3–5% upper crustal contamination and ~2% lower crustal contamination with the least contaminated sample having 1.2% upper crustal contamination (Fig. 10).

Mantle sources of the high-Ti group and degrees of partial melting

Magmas from which the high-Ti group was generated were relatively uncontaminated, and thus samples of this group are the most suitable for examining mantle source compositions. The dynamic melting inversion (DMI) method established by Zou and Zindler (1996) provides an effective means of estimating the source composition

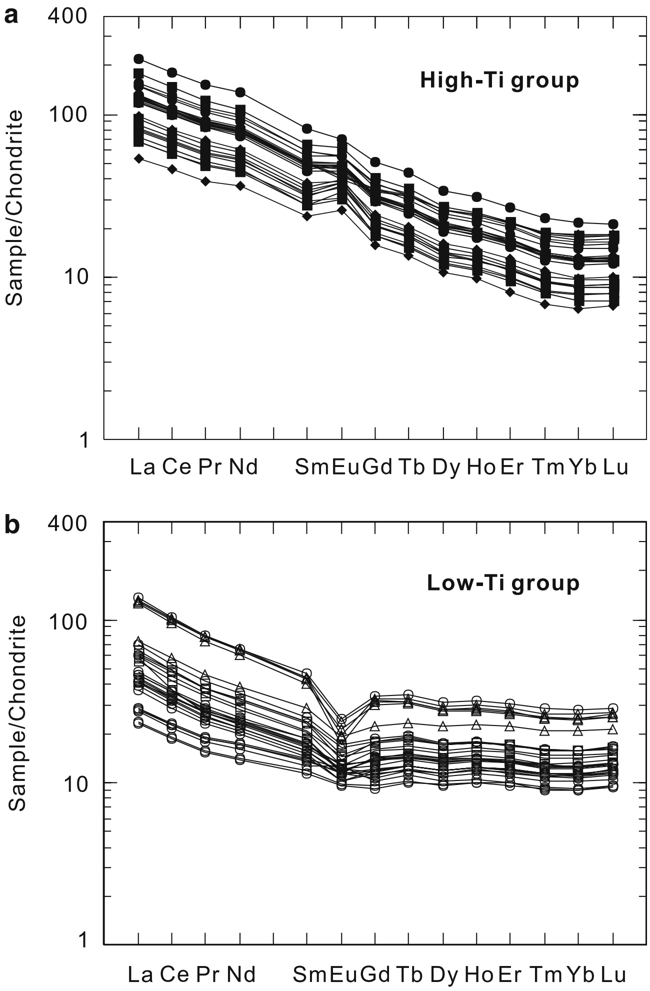

Fig. 6 Chondrite-normalized REE patterns for the mafic rocks of the high-Ti group (**a**) and low-Ti group (**b**) in Funing, SW China

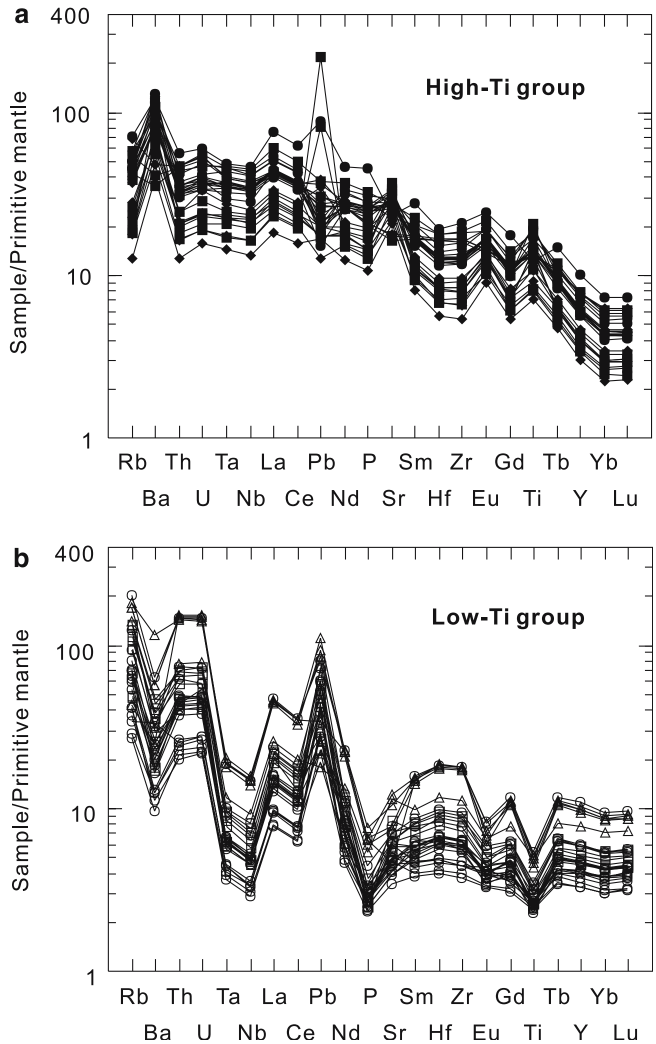

Fig. 7 Primitive mantle-normalized incompatible element patterns for the mafic rocks of the high-Ti group (**a**) and low-Ti group (**b**) in Funing, SW China. Normalization values are from Sun and McDonough (1989)

of mafic rocks and their degrees of partial melting (Zou et al. 2000). Based on the dynamic melting model, the source composition and degrees of partial melting can be determined independently without assuming one, in order to calculate the other. Therefore, the results obtained are expected to reflect more accurately the melting process. According to Zou et al. (2000), requirements for applying this method include: (1) the selected mafic rocks should have the same isotopic composition; (2) highly incompatible elements in general are used as a reference because their ratios with less-highly incompatible elements should be large and variable, implying that the selected samples formed from different degrees of partial melting; (3) the ratios of various element abundances (R) should vary systematically according to their bulk distribution coefficients; and (4) samples selected should represent liquid compositions typically with high Mg#. The high-Ti Shadou and Anding sills are un-differentiated. This interpretation is confirmed by the narrow range of REE concentrations in the high-Ti rocks. Thus their weighted mean concentrations can represent the liquid compositions. Therefore, the mean concentrations of trace elements, La, Ce, Nd, Sm, and Tb, are used for modeling (Table 4). Eu was not used for the calculations because it is sensitive to plagioclase fractionation during evolution of the magmas.

The concentration ratios (Q_a) of a highly incompatible element La with a less incompatible element Ce (Q_b) are as follows:

$$Q_a = Q_{La} = 27.61/12.51 = 2.207$$

$$Q_b = Q_{Ce} = 59.94/27.71 = 2.163$$

Applying these trace element ratios to the equations of Zou et al. (2000), degrees of partial melting are obtained for Anding and Shadou magmas of 6.32 (*f1*) and 8.21 (*f2*), respectively. Similarly, using La concentration ratio Q_a as a reference and Nd, Sm, and Tb to obtain Q_b, we obtained additional three sets of *f1* and *f2* values (Table 4). Thus, the source compositions of these

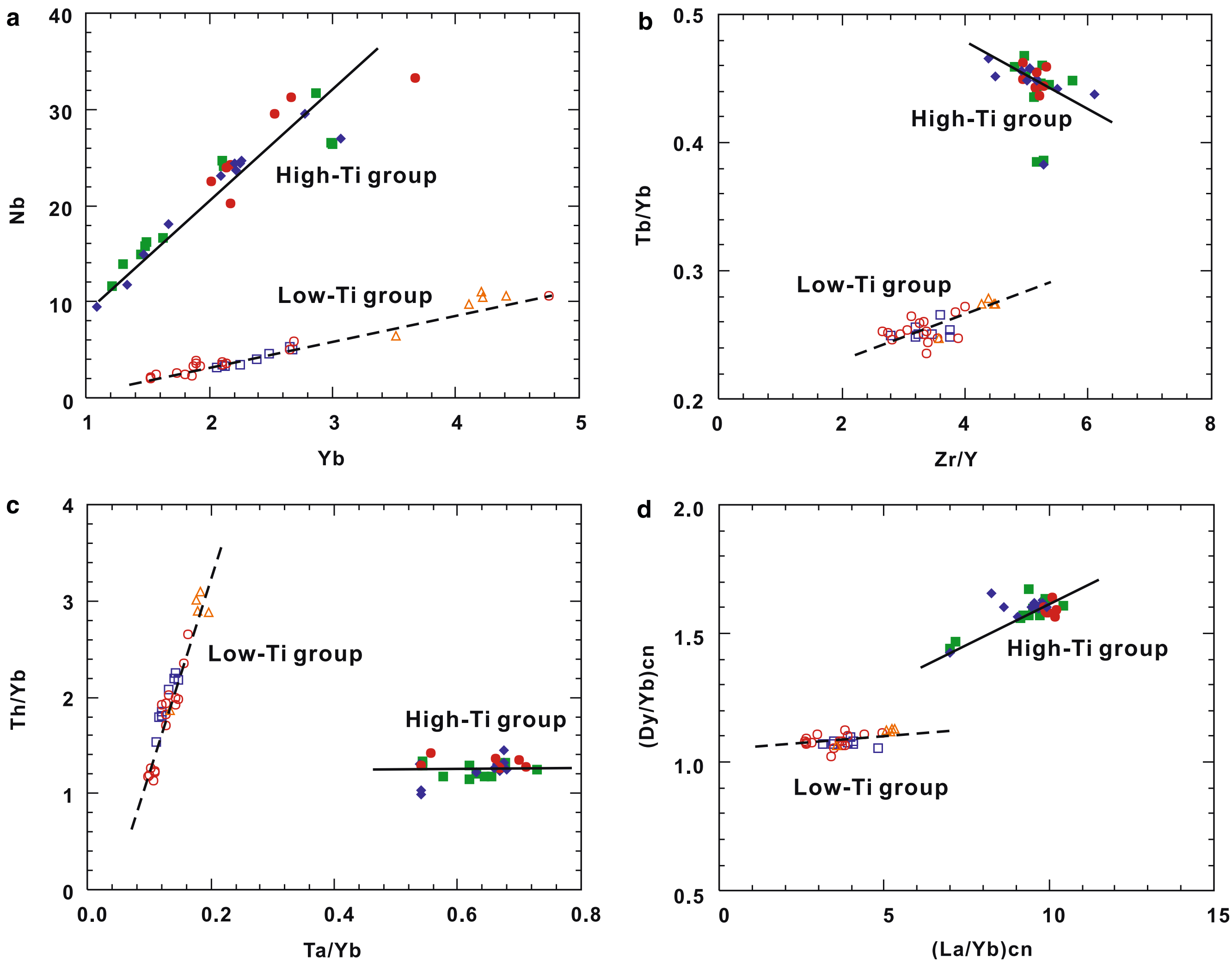

Fig. 8 Plots of the mafic rocks from Funing, Yunnan Province, SW China: (**c**) Yb versus Nb; (**d**) Zr/Y versus Tb/Yb; (**a**) Ta/Yb versus Th/Yb; and (**b**) (La/Yb)cn versus (Dy/Yb)cn

elements were obtained according to the method of Zou et al. (2000).

The calculated compositions of the mantle source for the rocks of both Shadou and Anding are LREE-enriched (Table 4). The magmas from which the Shadou and Anding rocks formed were generated by different degrees of partial melting: the high-Ti magmas of Shadou were formed by 9.5% melting whereas the high-Ti

Table 4 Mantle source compositions and degrees of partial melting for the Shadou and Anding mafic intrusions

Element	Bulk D	Anding	Shadou	*Q*	f_1 (%)	f_2 (%)	C_0	$(C_0)_{cn}$	$(C_0)_{pm}$
La	0.0021	34.7	25.9	1.33904			2.255	9.51	3.28
Ce	0.0041	74.7	56.1	1.33264	6.32	8.21	4.869	7.96	2.74
Nd	0.0095	42.8	32.6	1.31371	6.93	9.01	2.842	6.09	2.10
Sm	0.018	8.45	6.64	1.27319	7.12	9.26	0.595	3.89	1.34
Tb	0.033	1.11	0.90	1.24078	8.73	11.41	0.090	2.40	0.83
Ave.f					7.28	9.47			

Bulk D bulk distribution coefficients; *Q* concentration ratio = weighted mean concentration (ppm) of the Anding dyke divided by weighted mean concentration (ppm) of the Shadou sill; *f1* degree of partial melting for the Anding dyke; *f2* degree of partial melting for the Shadou sill; C_0 composition of the source; $(C_0)_{cn}$ chondrite-normalized source composition, $(C_0)_{pm}$ primitive mantle-normalized source composition; REE abundances of chondrite and primitive mantle are from Sun and McDonough (1989). Bulk partition coefficients and source mineral proportions are referenced from Zou and Zindler (1996). Source volume porosity $\phi = 1\%$, $\Phi = \rho_f \phi/(\rho_f \phi + \rho_s (1 - \phi))$, $\rho_f = 2.8$ g/cm^3, $\rho_s = 3.3$ g/cm^3. Calculation equations for the dynamic melting and bulk partition coefficients are from Zou et al. (2000)

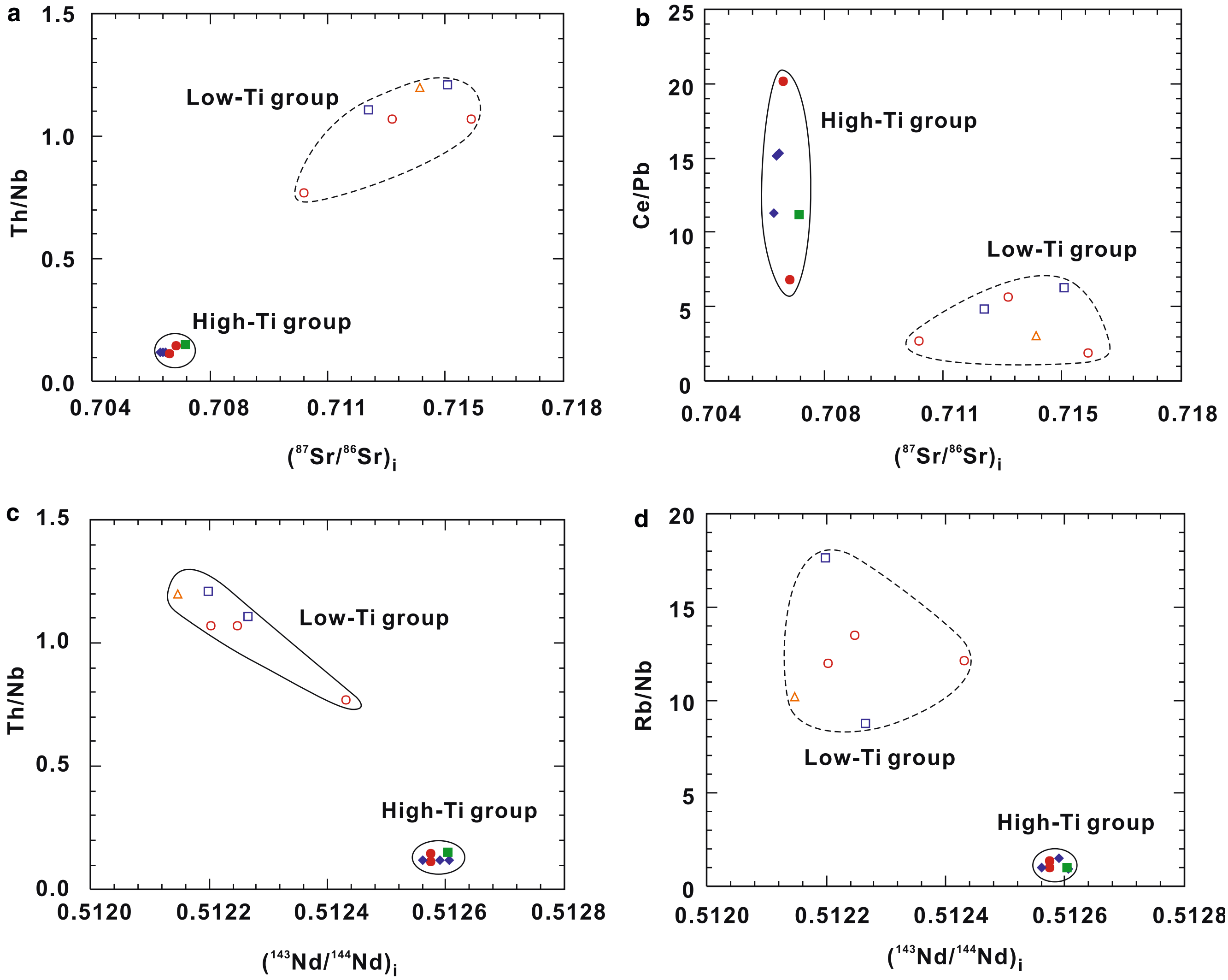

Fig. 9 Plots of ($^{87}Sr/^{86}Sr$)$_i$ versus Th/Nb (**a**) and Ce/Pb ratios (**b**) and ($^{143}Nd/^{144}Nd$)$_i$ versus Th/Nb (**c**) and Rb/Nb ratios (**d**) for the mafic rocks in Funing, Yunnan Province, SW China

magmas of Anding were formed by 7.3% melting. These magmas were little modified by interaction with continental crust.

An integrated petrogenetic model

The high-Ti group has a limited range of Sr and Nd isotopic ratios and highly enriched LREE, TiO_2, and P_2O_5. The high La/Yb ratios and the depletion of HREE can be explained by partial melting in the garnet stable field. These features are thus consistent with the derivation from an enriched, asthenospheric, OIB-type mantle source, supporting an origin related to a mantle plume.

Rocks of the high-Ti group have higher alkalis (Na_2O) and LREE than rocks of the low-Ti group. Therefore, both the low- and high-Ti groups cannot be generated from the same magma, because crustal contamination as recorded in the low-Ti group should increase the alkaline and LREE components. Crustal contamination of normal mantle-derived magmas during magma emplacement cannot explain the observed isotopic and geochemical differences between the low- and high-Ti groups from a consideration of mass balance. The much lower La/Yb ratios and relatively flat HREE suggest derivation of the low-Ti group from a shallow, lithospheric, enriched mantle. An enriched EM2-like source is proposed for the generation of the low-Ti group. An EM2-like source is usually explained to have formed by the previous subduction (Weaver 1991). The Yangtze Block was surrounded by oceanic subduction in Neoproterozoic time (Zhou et al. 2002a). A similar EM2-like mantle source has also been invoked for the Emeishan flood basalts (Song et al. 2001).

Field relationships indicate that the high-Ti sills/dykes are older than the low-Ti intrusions (e.g., Wu et al. 1963). Their new SHRIMP zircon U–Pb ages are

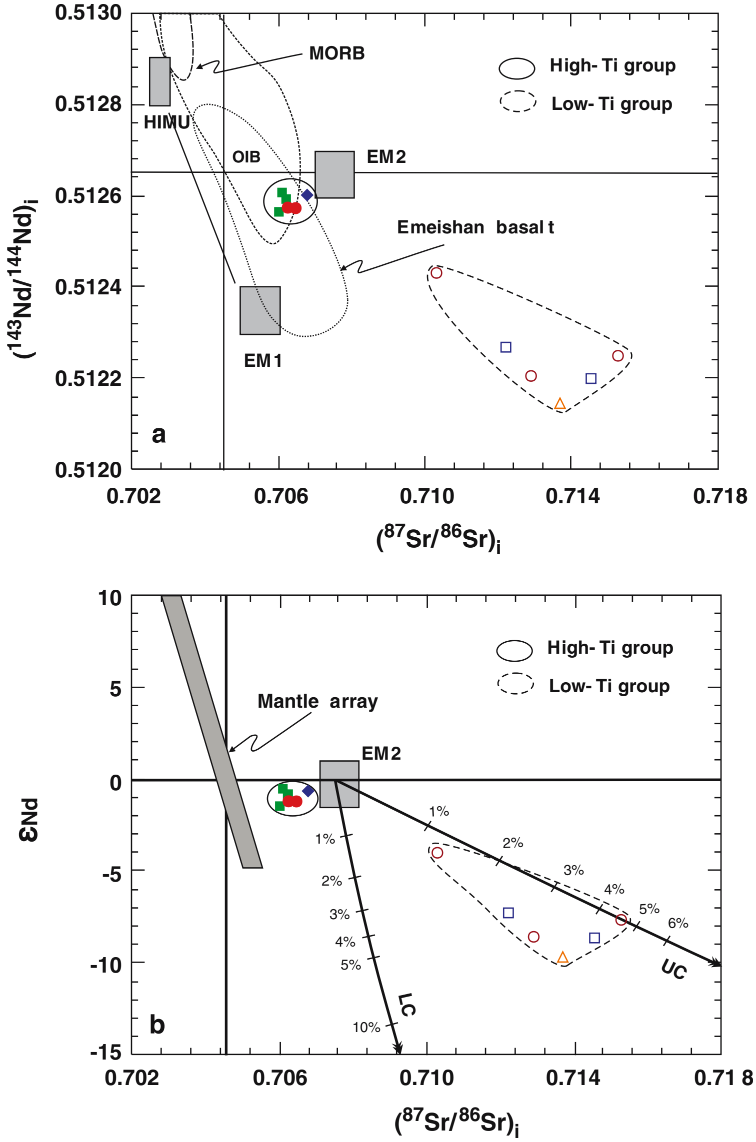

Fig. 10 Plots of $(^{143}Nd/^{144}Nd)_i$ versus $^{87}Sr/^{86}Sr_i$ (**a** and **b**) and modeling of crustal contamination of the mafic rocks in Funing, SW China. Field of the Emeishan flood basalts are based on data from Chung and Jahn (1995), Xu et al. (2001), Xiao et al. (2003), and Song et al. (2004). Fields of mantle array, *MORB, EM1, EM2, HIMU, UC* (*upper crust*) and LC (*lower crust*) are from Hart (1988) and Weaver (1991)

also supportive of such age relationship, although both types of intrusions have ages within their uncertainties (Fig. 2). It is therefore believed that the heat source needed for the melting of the lithospheric mantle was provided by a mantle plume.

Implications for ELIP magmatism

On the basis of geological correlations, the Emeishan flood basalts have a well-constrained age of end-Guadalupian (~260 Ma) (Yin et al. 1992; Jin and Shang 2000), although radiogenic dates for volcanic rocks are not available, because of post-eruption alteration and metamorphism (Boven et al. 2002; Ali et al. 2004). This eruptive age is consistent with SHRIMP zircon U–Pb ages of 259 ± 3 Ma for the Xinjie mafic–ultramafic intrusion near Miyi (Zhou et al. 2002b) and 262 ± 2 Ma for an olivine gabbroic dyke near Panzhihua (Guo et al. 2004).

Although mafic rocks in Funing were not previously considered to be part of the ELIP, the new SHRIMP zircon ages presented here for the Shadou and Anding intrusions are similar to ages for the ELIP elsewhere. The geochemistry of the volcanic rocks in Funing is identical to the diorite of the layered intrusions. They are broadly comparable to low-Ti basalts of the ELIP elsewhere, although they show heavier crustal contamination. In the absence of any other known magmatism of this age and composition in the region, it is suggested that the mafic rocks in Funing were produced by the same mantle plume that generated the ELIP. Much of SW China is covered by Triassic strata and it is possible that large portions of the ELIP are not exposed (Yan et al. 2003). If so, the real extent of the ELIP would be much greater than previously thought, perhaps on the

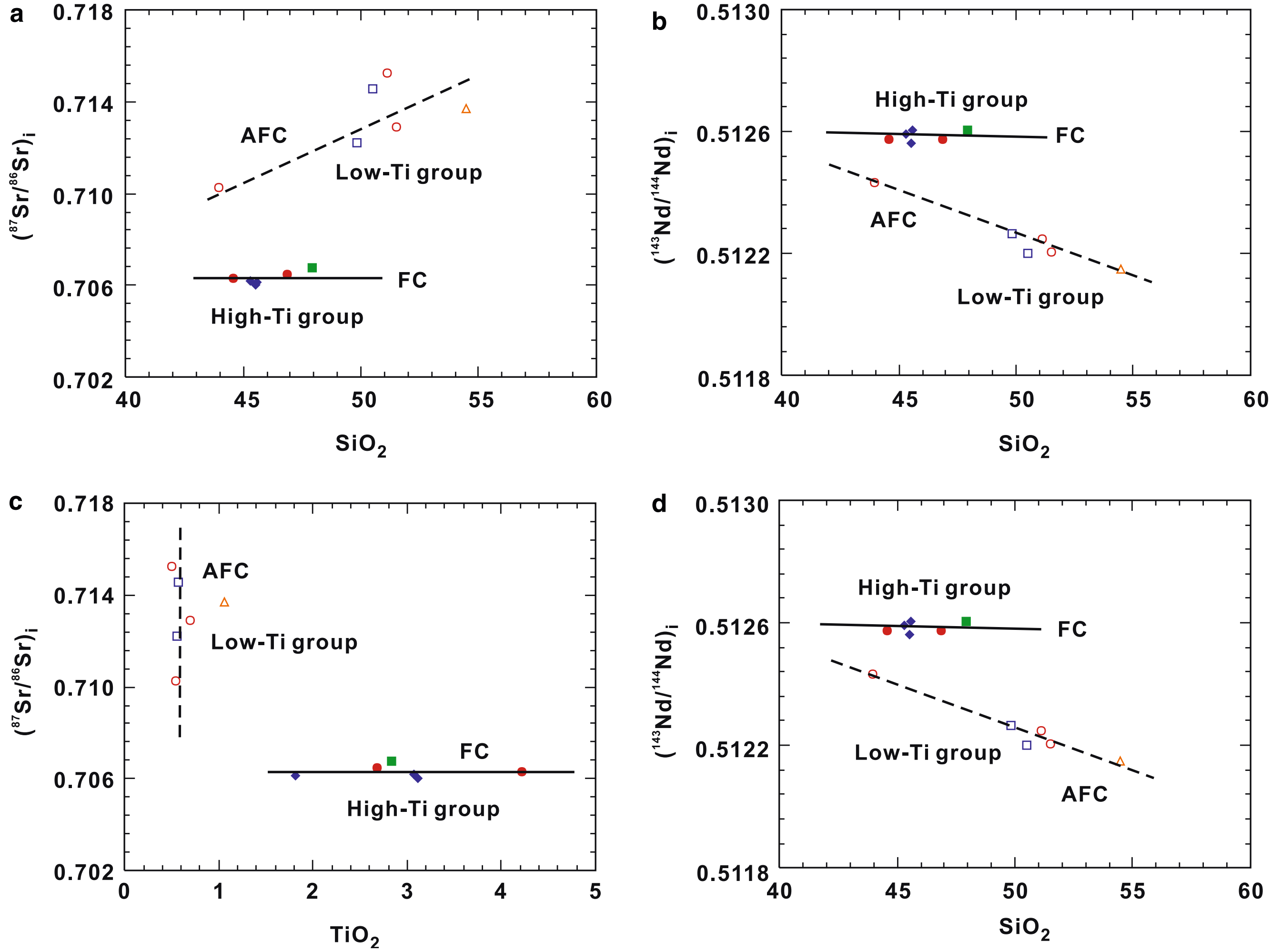

Fig. 11 Plots of SiO_2 versus ($^{87}Sr/^{86}Sr)_i$ (**a**) and ($^{143}Nd/^{144}Nd)_i$ ratios (**b**) and TiO_2 versus ($^{87}Sr/^{86}Sr)_i$ (**c**) and ($^{143}Nd/^{144}Nd)_i$ ratios (**d**) for the mafic rocks in Funing, Yunnan province, SW China. *FC*, fractional crystallization; and *AFC*, assimination and fractional crystallization

order of 1×10^6 km^2 (Song et al. 2004). This interpretation extends the inferred distribution of the ELIP and supports our contention that a major igneous event took place at ~260 Ma.

Mafic–ultramafic intrusions in the ELIP are spatially and temporally associated with the Emeishan flood basalts, which include both high- and low-Ti varieties (Xu et al. 2001) and alkaline rocks (Ma et al. 2003). Although genetic links between the intrusive and extrusive suites within the ELIP have not yet been established, the low-Ti-layered intrusions in Funing are geochemical analogies to the volcanic rocks, strongly supporting the interpretation of a similar origin. The same mantle plume is therefore believed to have been responsible for the formation of the entire suite.

The identification of both the low- and high-Ti groups in Funing suggests a diversity in the plutonic rocks, similar to that of the volcanic rocks of the ELIP. The diversity of plutonic rocks in Funing is similar to that of the Siberian Traps, which contain alkaline complexes and tholeiitic and picritic intrusions associated with flood basalts. Intrusions in the Noril'sk-Talnakh region of Siberia with distinctive petrology and chemical compositions are considered to have formed from magmas of variable composition (Naldrett et al. 1992; Lightfoot et al. 1990; 1993; Fedorenko and Czamanske 1997; Arndt et al. 1993, 1998), produced from mantle-derived melts that experienced different degrees of crustal contamination (Naldrett et al. 1992; Lightfoot et al. 1993, 1994; Arndt et al. 2003). Similarly, geochemical differences between the two types of intrusions in the Funing area indicate that a variety of processes were involved in the formation of the ELIP. These involved not only a rising mantle plume that transported mass and energy from the asthenospheric mantle to the continental crust but also extensive crustal contamination and derivation from enriched mantle source regions.

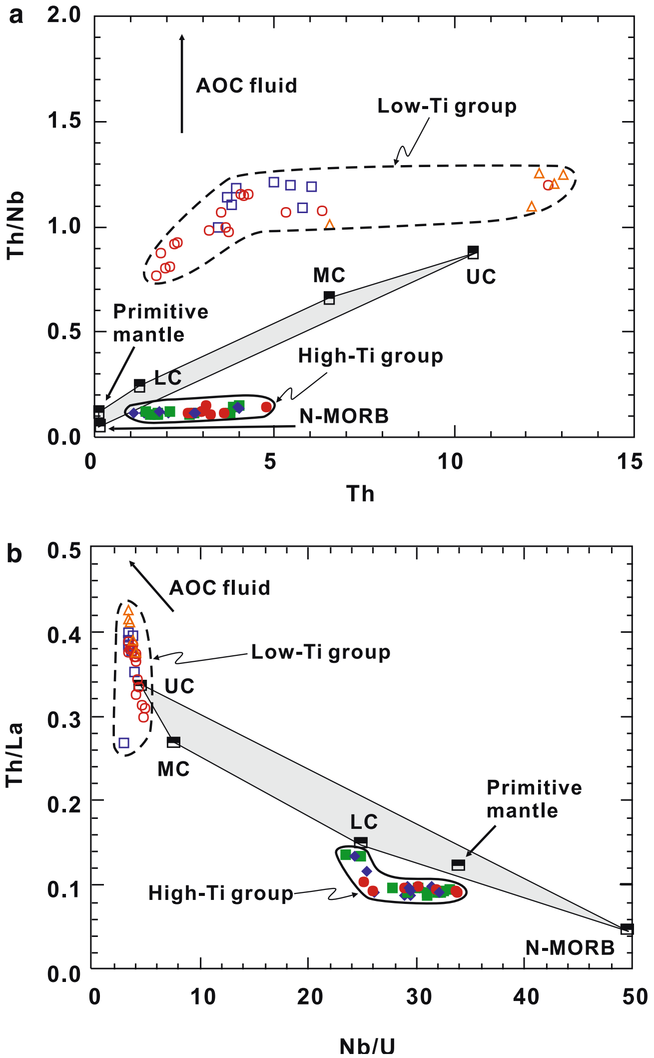

Fig. 12 Plots of the mafic rocks from Funing, Yunnan Province, SW China: **a** Th versus Th/Nb and **b** Th/La versus Nb/U. Values of *lower crust* (LC), *middle crust* (MC), and *upper crust* (UC) are from Rudnick and Gao (2003), N-MORB and primitive mantle from Sun and McDonough (1989) and *altered oceanic fluids* (AOF) from Dorendorf et al. (2000)

Conclusions

The ELIP is composed of the Emeishan flood basalts and a variety of mafic–ultramafic intrusions. The intrusions have compositions and isotopic signatures similar to those of the volcanic rocks, indicating derivation from the same mantle source. The Funing intrusions include high- and low-Ti groups, have ages identical to those of ELIP plutonic bodies and the associated volcanic rocks, and show the same diversity of compositions as the Emeishan flood basalts, strongly suggesting that they are all part of the same magmatic event at ~260 Ma. The high-Ti group in Funing formed from relatively uncontaminated mafic melts produced by low degrees of partial melting of an enriched, OIB-type, asthenospheric mantle source an EM2-like source and was, whereas the low-Ti group was derived from heavily crustally contaminated. These two melt types then evolved along different paths by FC.

Acknowledgements This study was supported by an outstanding young researcher award from the National Nature Science Foundation of China (Project 40129001), and a matching fund from The University of Hong Kong (to M. F. Zhou). The study was also supported by grant from the Research Grant Council of Hong Kong, China (HKU7056/03P and HKU7057/05P). We thank Ms. Xiao Fu for assistance with sample analyses, Mr. Wei-Hua Sun and Mr. Xiao-Ping Xia for assistance with the preparation of this manuscript and Dr. Allen Kennedy for SHRIMP analyses. Reviews by Peter C. Lightfoot and an anonymous referee improved an early draft of this paper and are gratefully acknowledged.

References

Ali JR, Lo CH, Thompson GM and Song XY (2004) Emeishan basalt Ar–Ar overprint ages define several tectonic events that affected the western Yangtze platform in the Mesozoic and Cenozoic. J Asian Earth Sci 23:163–178

Arndt NT, Czamanske GK, Wooden JL, Fedorenko VA (1993) Mantle and crustal contributions to continental flood volcanism. Tectonophysics 223: 39–52

Arndt NT, Chauvel C, Fedorenko V, Czamanske G (1998) Two mantle sources, two plumbing systems: tholeiitic and alkaline magmatism of the Maymecha River basin, Siberian flood volcanic province. Contrib Mineral Petrol 133: 297–313

Arndt NT, Czamanske GK, Walker RJ, Chauvel C, Fedorenko VA (2003) Geochemistry and origin of the intrusive hosts of the Noril'sk-Talnakh Cu-Ni-PGE sulfide deposits. Econ Geol 98: 495–515

Boven A, Pasteelsa AP, Punzalana LE, Liu BJ, Luoa X, Zhang BW, Guo BZ, Hertogen CJ (2002) $^{40}Ar/^{39}Ar$ geochronological constraints on the age and evolution of the Permo-Triassic Emeishan volcanic province, Southwest China. J Asian Earth Sci 20: 157–175

Chung SL, Jahn BM (1995) Plume-lithosphere interaction in generation of the Emeishan flood basalts at the Permian-Triassic boundary. Geology 23: 889–892

Claoue-Long JC, Zhang Z, Ma G, Du S (1991) The age of Permian-Triassic boundary. Earth Planet Sci Lett 105: 182–190

Compston W, Williams IS, Meyer C (1984) U-Pb geochronology of zircons from Lunar Breccia 73217 using a sensitive high mass-resolution ion microprobe. J Geophys Res 89: 525–534

Dorendorf F, Wiechert U, Worner G (2000) Hydrated sub-arc mantle: a source fpr the Kluchevskoy volcano, Kamchatka/Russia. Earth Planet Sci Lett 175: 69–86

Fedorenko VA, Czamanske GK (1997) Results of new field and geochemical studies of the volcanic and intrusive rocks of the Maymecha-Kotuy area, Siberian flood-basalt province, Russia. Int Geol Rev 39: 479–531

Guo F, Fan WM, Wang Y, Li C (2004) When did the Emeishan mantle plume activity start?: Geochronological and geochemical evidence from ultramafic-mafic dikes in Southwestern China. Int Geol Rev 46: 226–234

Hanski E, Walker RJ, Huhma H, Polyakov GV, Balykin PA, Hoa TT, Phuong NT (2004) Origin of the Permian-Triassic komatiites, northwestern Vietnam. Contrib Mineral Petrol 147: 453–469

Hart SR (1988) Heterogeneous mantle domains: signature, genesis and mixing chronologies. Earth Planet Sci lett 90: 273–296

Jin Y, Shang J. (2000) The Permian of China and its interregional correlation. In: Yin H, Dickins JM, Shi GR, Tong J (eds) Permian-Triassic evolution of Tethys and western Circum-Pacific: developments in Palaeontology and Stratigraphy 18, Elsevier Press, Amsterdam, pp 71–98

Lightfoot PC, Naldrett AJ, Gorbachev NS, Doherty W, Fedorenko VA (1990) Geochemistry of the Siberian Trap of the Norilsk area, USSR, with implications for the relative contributions of crust and mantle to flood-basalt magmatism. Contrib Mineral Petrol 104: 631–644

Lightfoot PC, Hawkesworth CJ, Hergt J, Naldrett AJ, Gorbachev NS, Fedorenko VA, Doherty W (1993) Remobilization of the continental lithosphere by a mantle plume - major-element, trace-element, and Sr-isotope, Nd-isotope, and Pb-isotope evidence from picritic and tholeiitic lavas of the Norilsk district, Siberian Trap, Russia. Contrib Mineral Petrol 114: 171–188

Lightfoot PC, Hawkesworth CJ, Hergt J, Naldrett AJ, Gorbachev NS, Fedorenko VA, Doherty W (1994) Chemostratigraphy of Siberian trap lavas, Noril'sk district, Russia: implications for the evolution of flood basalt magmas. In: Lightfoot PC, Naldrett AJ (eds) Proceedings of the Sudbury-Noril'sk Symposium. Ont Geol Surv Spec Vol 5, pp 283–312

Ma YX, Ji XT, Li JC, Huang M, Min ZZ (2003) Mineral resources of Panzhihua, Sichuan Prvince, SW China. Chengdu University of Technology, pp 275

Naldrett AJ (2004) Magmatic sulfide deposits—geology, geochemistry and exploration. Springer, Berlin, Heidelberg, New York, pp 727

Naldrett AJ, Lightfoot PC, Fedorenko V, Doherty W, Gorbachev NS (1992) Geology and geochemistry of intrusions and flood basalts of the Noril'sk region, USSR, with implications for the origin of the Ni–Cu ores. Econ Geol 87: 975–1004

Qi L, Hu J, Gregoire DC (2000) Determination of trace elements in granites by inductively coupled plasma–mass spectrometry. Talanta 51: 507–513

Rollison H (1993) Using geochemical data: evaluation, presentation, interpretation. Longman, Singapore, pp 352

Rudnick RL, Gao S (2003) Composition of the continental crust. In: Holland HD, Turekian KK (eds) The Crust (ed. RL Rudnick) Vol. 3, Treatise on Geochemistry, Elsevier, Oxford. pp1–64

Song XY, Zhou M-F, Hou ZQ, Cao Z, Wang Y, Li Y (2001) Geochemical constraints on the mantle source of the Upper Permian Emeishan continental flood basalts, southwestern China. Int Geol Rev 43: 213–225

Song XY, Zhou M-F, Cao ZM, Sun M (2003) Ni–Cu–(PGE) magmatic sulfide deposits in the Yangliuping area, Permian Emeishan igneous province, SW China. Mineralium Deposita 38: 831–843

Song XY, Zhou M-F, Cao Z, Robinson PT (2004) Late Permian rifting of the South China Craton caused the Emeishan mantle plume. J Geol Soc 161: 773–781

Sun SS, McDonough WF (1989) Chemical and isotopic systematics of oceanic basalts: implications for mantle composition and processes. In: Saunders A. D. and Norry M.J. (eds.), Magmatism in the ocean basins. Geol Soc Spec Publ 42: 313–345

Weaver BL (1991) The origin of ocean island basalt end-member compositions: trace element and isotopic constraints. Earth Planet Sci Lett 104: 381–397

Wu LR, Liu RX, Mei HJ, Xiao SH (1963) Mafic rocks and Ni–Cu sulfide deposits in Funing, Yunnan. Unpubl. Report of Chinese Academy of Sciences (in Chinese)

Xiao L, Xu Y, Chung SL, He B, Mei H (2003) Chemostratigraphic correlation of Upper Permian lavas from Yunnan Province, China: extent of the Emeishan large igneous province. Int Geol Rev 45: 753–766

Xu YG, Chung SL, Jahn BM, Wu GY (2001) Petrologic and geochemical constraints on the petrogenesis of Permian-Triassic Emeishan flood basalts in southwestern China. Lithos 58: 145–168

Yan DP, Zhou M-F, Song HL, Wang XW, Malpas J (2003) Origin and tectonic significance of a Mesozoic multi-layer over-thrust within the Yangtze Block (South China). Tectonophysics 361: 239–254

YBGMR (Yunnan Bureau of Geology and Mineral Resources) (1990) Regional geology of Yunnan Province. Geological Memoirs, MGMR, S.1, N.21 (in Chinese). Geological Publishing House, Beijing, pp 554

Yin A, Nie S (1996) A Phanerozoic palinspastic reconstruction of China and its neighboring region. In: Yin A, Harrison TM (eds) The tectonic evolution of Asia. Cambridge University Press, New York, pp 442–85

Yin H, Huang S, Zhang K, Hansen HJ, Yang F, Ding M, Bie X (1992) The effects of volcanism of the Permo-Triassic mass extinction in South China, In: Sweet W.C., Yang Z.Y., Dickins J.M. and Yin H. F. (eds.), Permo-Triassic Events in the Eastern Tethys: Stratigraphy, Classification, and Relations with the Western Tethys. World and Regional Geology, v.2. Cambridge University Press, Cambridge, pp 146–157

Zhang HF, Sun M, Lu FX, Zhou XH, Zhou M-F, Liu YS, Zhang GH (2001) Moderately depleted lithospheric mantle underneath the Yangtze Block: evidence from a garnet lherzolite xenolith in the Dahongshan kimberlite. Geochem J 35: 315–331

Zhong H, Zhou XH, Zhou MF, Sun M, Liu BG (2002) Platinum-group element geochemistry of the Hongge layered intrusion in the Pan-Xi Area, Southwestern China. Mineralium Deposita 37: 226–239

Zhou M-F, Yan DP, Kennedy AK, Li YQ, Ding J (2002a) SHRIMP zircon geochronological and geochemical evidence for Neoproterozoic arc-related magmatism along the western margin of the Yangtze Block, South China. Earth Planet Sci Lett 196: 51–67

Zhou M-F, Malpas J, Song X, Kennedy AK, Robinson PT, Sun M, Lesher CM, Keays RR (2002b) A temporal link between the Emeishan large igneous province (SW China) and the end-Guadalupian mass extinction. Earth Planet Sci Lett 196: 113–122

Zhou M-F, Yang ZX, Song XY, Lesher CM, Keays RR (2002c) Magmatic Ni-Cu-(PGE) sulfide deposits in China In: Cabri LJ (ed) The geology, geochemistry, mineralogy, mineral beneficiation of the platinum-group elements. Canadian Institute of Mining, Metallurgy and Petroleum, Special vol 54, pp 619–636

Zhou M-F, Robinson PT, Lesher CM, Keays RR, Zhang C-J, Malpas J (2005) Geochemistry, petrogenesis, and metallogenesis of the Panzhihua gabbroic layered intrusion and associated Fe–Ti–V–oxide deposits, Sichuan Province, SW China. J Petrol 46:2253–2280

Zou HB, Zindler A (1996) Constraints on the degree of dynamic partial melting and source composition using concentration ratios in magma. Geochim Cosmochim Acta 60: 711–717

Zou HB, Zindler A, Xu XS, Qi Q (2000) Major, trace element, and Nd, Sr and Pb isotope studies of Cenozoic basalts in SE China: mantle sources, regional variations, and tectonic significance. Chem Geol 171: 33–47